Characterization of X-point radiation operational space and performance impact in DIII-D H-mode discharges

[1]F. Scotti, [2]A. Moser, [3]M. Bernert, [2]A. Leonard, [1]A. McLean, [4]M. Shafer, [3]U. Stroth, [2]N. Yadav, [1]M. Zhao, [2]C. Chrystal, [2]F. Conti, [1]M. Fenstermacher, [4]S. Gorno, [1]C. Lasnier, [1]T. Rognlien, [5]C. Tsui, [2]J. Yu, [2]H.Q. Wang

[1]Lawrence Livermore National Laboratory
[2]General Atomics
[3]Max Planck Institute for Plasma Physics
[4]Oak Ridge National Laboratory
[5]OakSandia National Laboratory

Fifth Technical Meeting on Divertor Concepts
IAEA Headquarters
October 28-31, 2025

DIII-D NATIONAL FUSION FACILITY

Lawrence Livermore National Laboratory

Regimes with X-point radiation considered for future reactors due to combination of detachment and ELM mitigation

- X-point radiator (XPR) scenarios initially developed in non-C devices ASDEX-Upgrade, JET with N, Ne, Ar seeding [Bernert NF21]
  - Deep XPR (Z_{rad}-Z_X~8 cm) leads to elimination of ELMs and reduction in confinement in AUG/JET [Bernert PSI24]
- XPR also obtained in C-devices (e.g., TCV) with increase flux expansion [Remeirdes NME24, Gorno PoP24, Lee PRL25], also with ELM mitigation

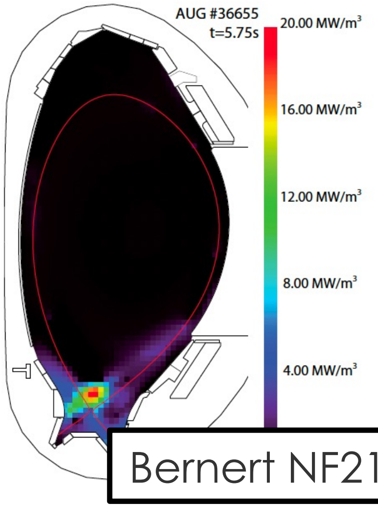

Bernert NF21

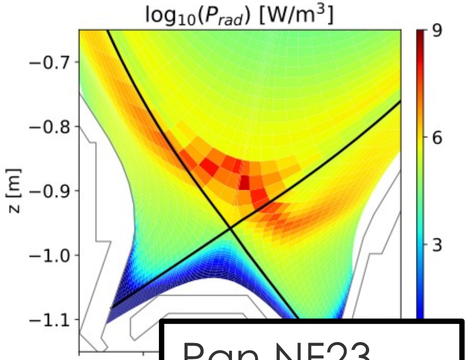

Pan NF23

DIII-D NATIONAL FUSION FACILITY

Regimes with X-point radiation considered for future reactors due to combination of detachment and ELM mitigation

- X-point radiator (XPR) scenarios initially developed in non-C devices ASDEX-Upgrade, JET with N, Ne, Ar seeding [Bernert NF21]
  - Deep XPR (Z_{rad}-Z_X~8 cm) leads to elimination of ELMs and reduction in confinement in AUG/JET [Bernert PSI24]
- XPR also obtained in C-devices (e.g., TCV) with increase flux expansion [Remeirdes NME24, Gorno PoP24, Lee PRL25], also with ELM mitigation
- Extrapolation of XPR to future devices needs predictive capabilities:
  - Impact on confinement, dilution, particle exhaust
  - Access and controllability of ELM mitigation
  - Validation of 2D and simple models for operational space

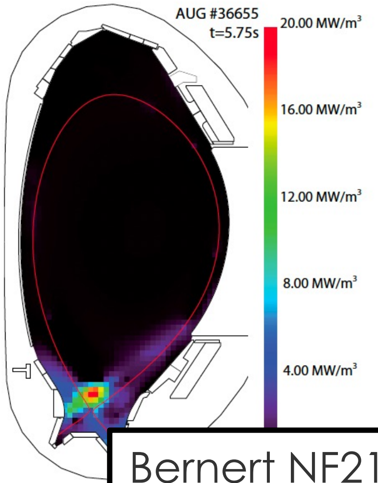

Bernert NF21

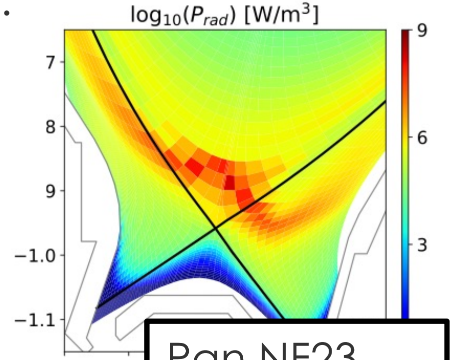

Pan NF23

X-point radiation generally observed in DIII-D discharges as evolution of deep detachment conditions with C, N, Ne radiators

- X-point radiation typically associated with:
  - confinement degradation
  - change in ELM behavior
  - eventually HL back transition
  - Sometimes MARFE evolution

- X-point radiation observed in both high and low δ H-mode discharges, snowflake, high-β_p, high-β hybrid scenarios
  - Advanced tokamak scenarios often able to offset XPR confinement loss with advanced high-performance core

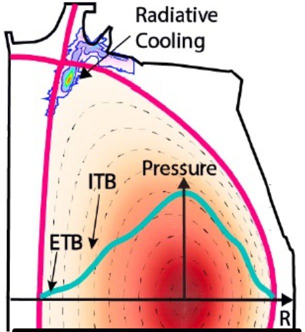

[Wang L, NC21]

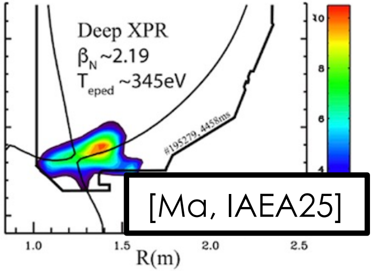

[Ma, IAEA25]

[Maingi FST05, Moser FEC23, Soukhanovskii NME24, Wang NC21, Wang, APS24]

X-point radiation generally observed in DIII-D discharges as evolution of deep detachment conditions with C, N, Ne radiators

- X-point radiation typically associated with:
  - confinement degradation
  - change in ELM behavior
  - eventually HL back transition
  - Sometimes MARFE evolution
- X-point radiation observed in both high and low δ H-mode discharges, snowflake, high-β_p, high-β hybrid scenarios
  - Advanced tokamak scenarios often able to offset XPR confinement loss with advanced high-performance core
- This work explores XPR access in standard H-mode towards validation of reduced XPR models
  - Characterization of operating space
  - 2D characterization of n_e, T_e, radiation front dynamics
  - Effect of XPR on transport, ELM suppression, confinement

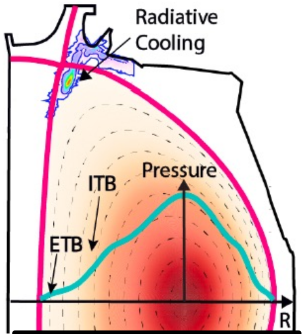

[Wang L, NC21]

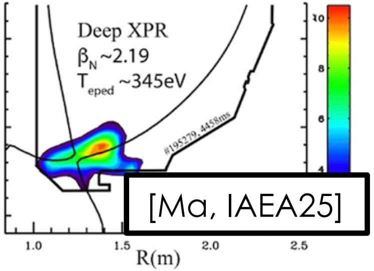

[Ma, IAEA25]

[Maingi FST05, Moser FEC23, Soukhanovskii NME24, Wang NC21, Wang, APS24]

Experiment performed in open divertor configuration for flexible shaping and optimal divertor diagnostic coverage

- Plasma current: 0.8-1.3 MA; Toroidal field: -2 T
- P_{aux}=6-12 MW (NBI: 6-9 MW, ECH: 0:3 MW)
- κ=1.75, δ_{top}, δ_{bot}=0.35
- Feed forward gas puffing:
  - D_2
  - CD_4 (PFR) 0-35 Torr l/s (for C fraction scan)
  - N_2 (PFR) 0-20 Torr l/s (for N-dominated $P_{rad\text{-}XPR}$)
- Medium, low, zero X-point height (12, 5, 0 cm)
- Divertor diagnostics:
  - DTS, bolometry, imaging, VUV/UV/VIS spectroscopy

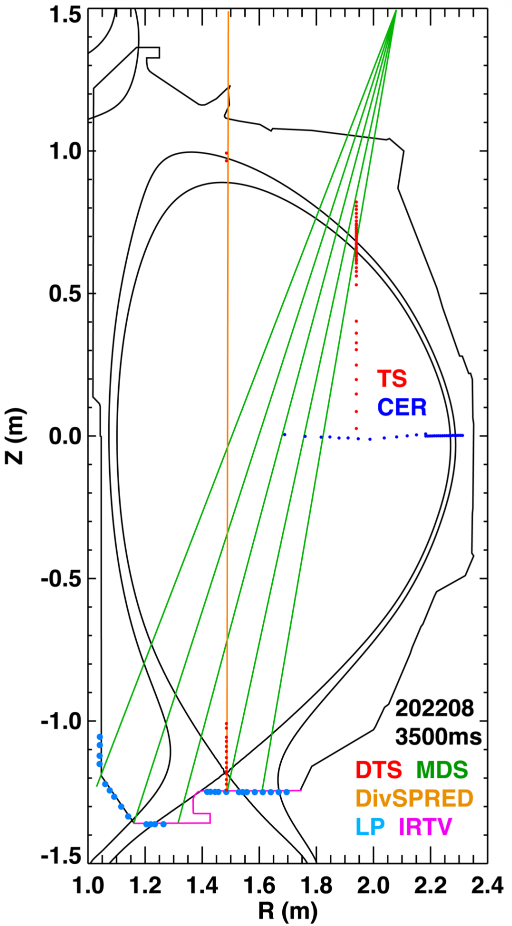

DIII-D NATIONAL FUSION FACILITY

X-point radiation accessed via PFR gas seeding leads to sustained ELM-mitigated phase

- Detachment accessed via deuterium fueling exploiting intrinsic C radiation

1	Attached
2	Detached
3	X-point Radiator (XPR)
4	HL dithering (XPR)
5	L-mode (XPR)

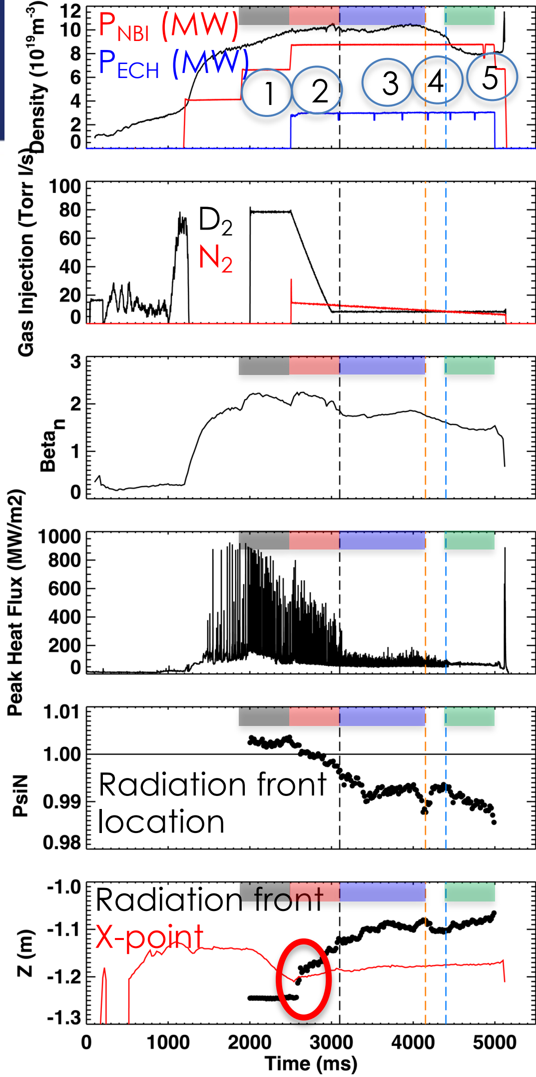

X-point radiation accessed via PFR gas seeding leads to sustained ELM-mitigated phase

- Detachment accessed via deuterium fueling exploiting intrinsic C radiation
- Impurity seeding (CD_4, N_2) used to push to X-point radiation
- As radiation front moves into confined plasma, ELM mitigation is observed with Type III ELMs

1	Attached
2	Detached
3	X-point Radiator (XPR)
4	HL dithering (XPR)
5	L-mode (XPR)

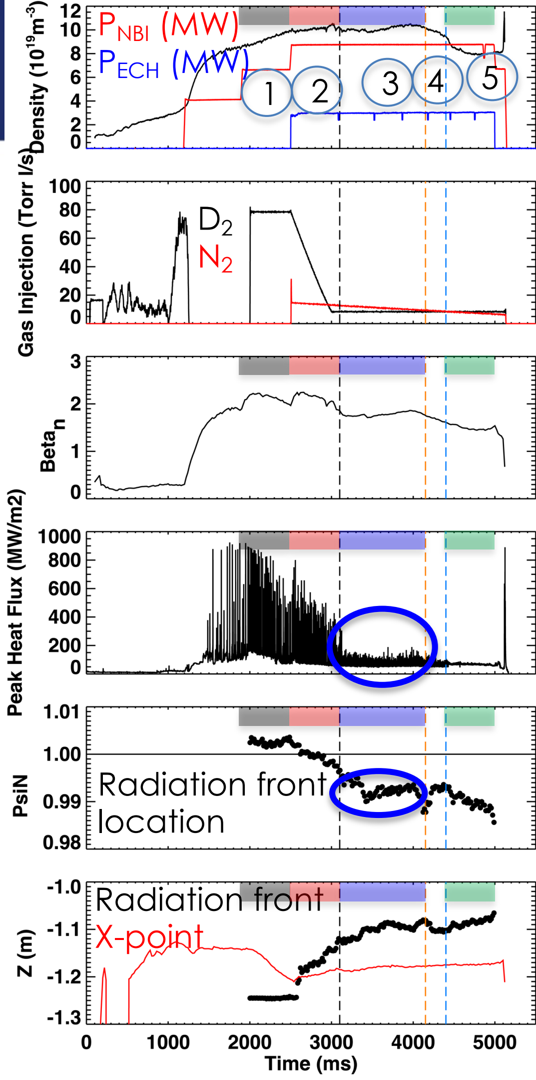

DIII-D NATIONAL FUSION FACILITY

X-point radiation accessed via PFR gas seeding leads to sustained ELM-mitigated phase

- Detachment accessed via deuterium fueling exploiting intrinsic C radiation
- Impurity seeding (CD_4, N_2) used to push to X-point radiation
- As radiation front moves into confined plasma, ELM mitigation is observed with Type III ELMs
- ELM mitigated phase followed by HL dithery phase and back-transition to L-mode
- No unstable MARFE evolution

1	Attached
2	Detached
3	X-point Radiator (XPR)
4	HL dithering (XPR)
5	L-mode (XPR)

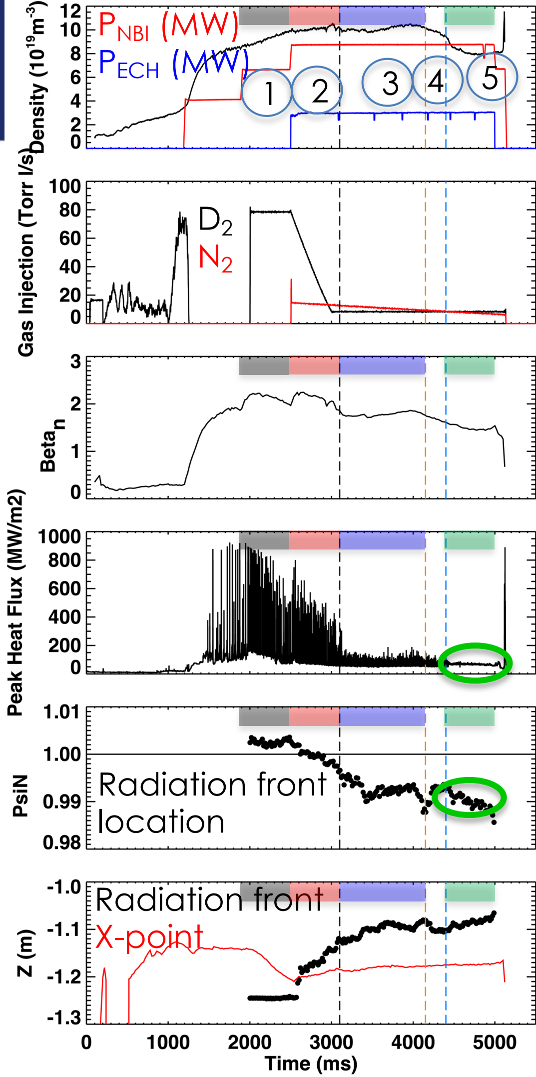

DIII-D NATIONAL FUSION FACILITY

Access to X-point radiation and ELM-mitigation associated with degradation (~20%) in pedestal performance (T_e, p_e)

- X-point radiation phase leads to reduced pedestal and separatrix T_e, p_e with nearly unchanged pedestal n_e structure
- XPR maintained in L-mode phase after loss of T_e, n_e pedestals

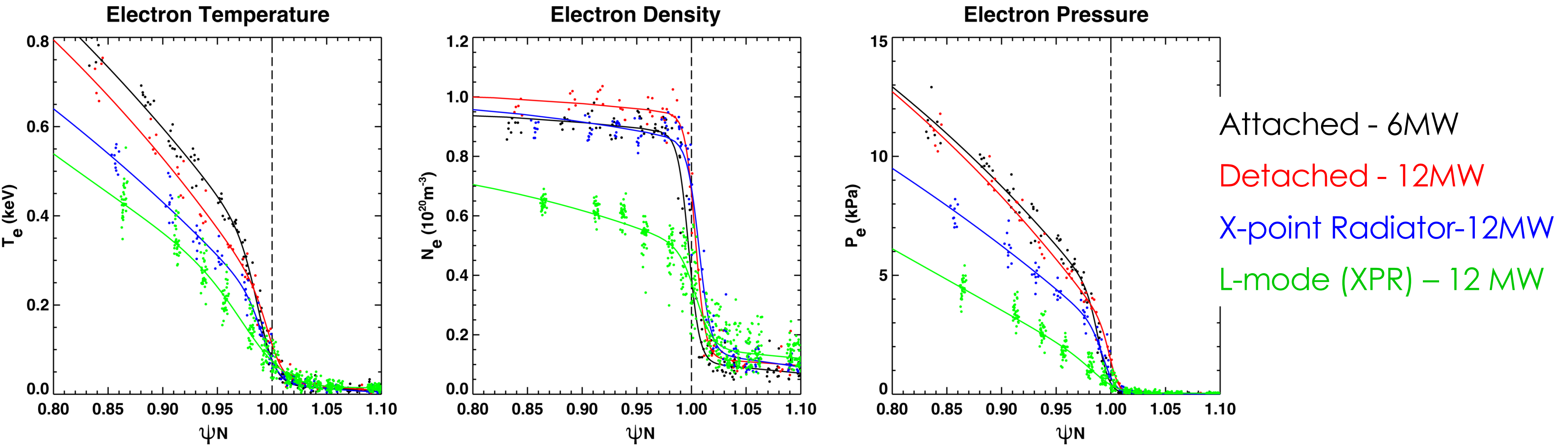

X-point radiation access with reduced pedestal and separatrix T_e, unchanged pedestal density but higher separatrix density

- Database of pedestal and separatrix values assembled across detached and XPR conditions in this experiment
  - Uncertainty in LCFS localization affects $n_{e\text{-}sep}$, $T_{e\text{-}sep}$ determination in XPR conditions

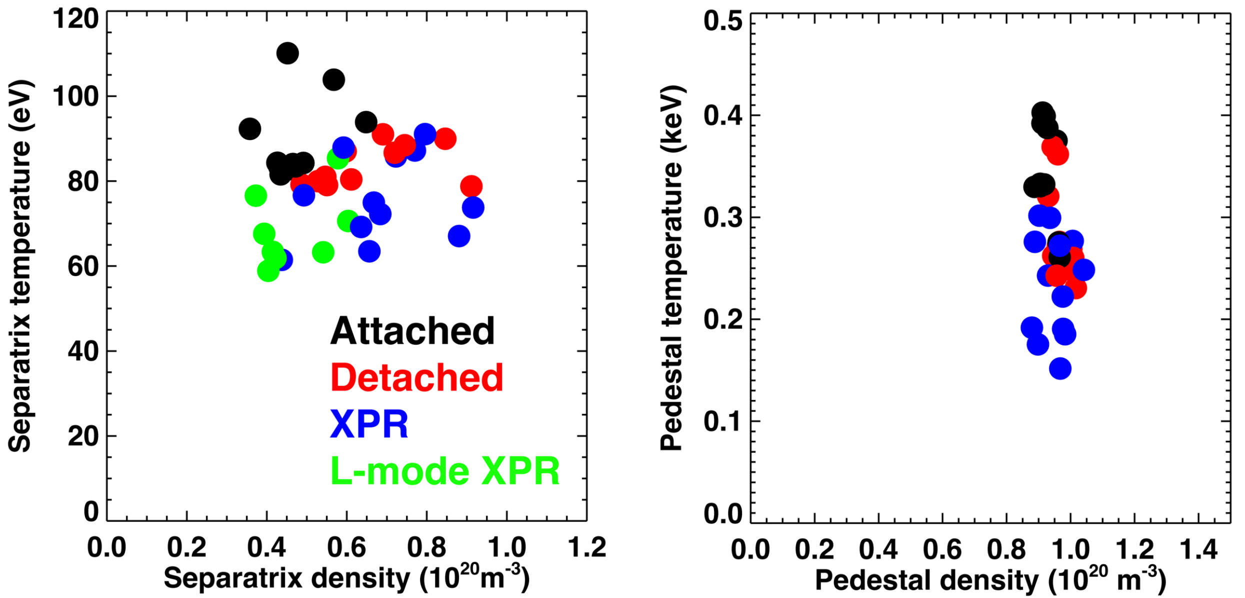

X-point radiation access with reduced pedestal and separatrix T_e, unchanged pedestal density but higher separatrix density

- Database of pedestal and separatrix values assembled across detached and XPR conditions in this experiment
  - Uncertainty in LCFS localization affects $n_{e\text{-}sep}$, $T_{e\text{-}sep}$ determination in XPR conditions

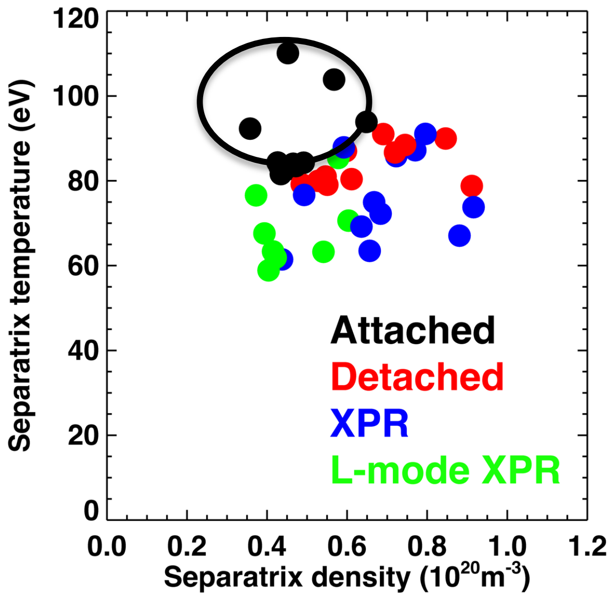

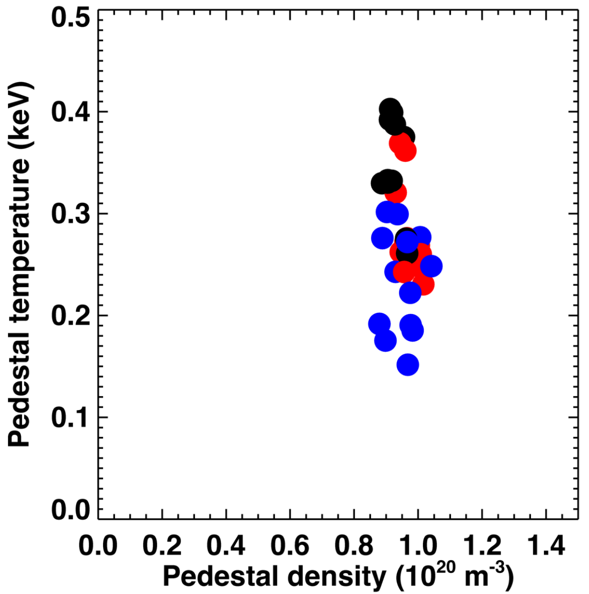

X-point radiation access with reduced pedestal and separatrix T_e, unchanged pedestal density but higher separatrix density

- Database of pedestal and separatrix values assembled across detached and XPR conditions in this experiment
  - Uncertainty in LCFS localization affects $n_{e\text{-}sep}$, $T_{e\text{-}sep}$ determination in XPR conditions

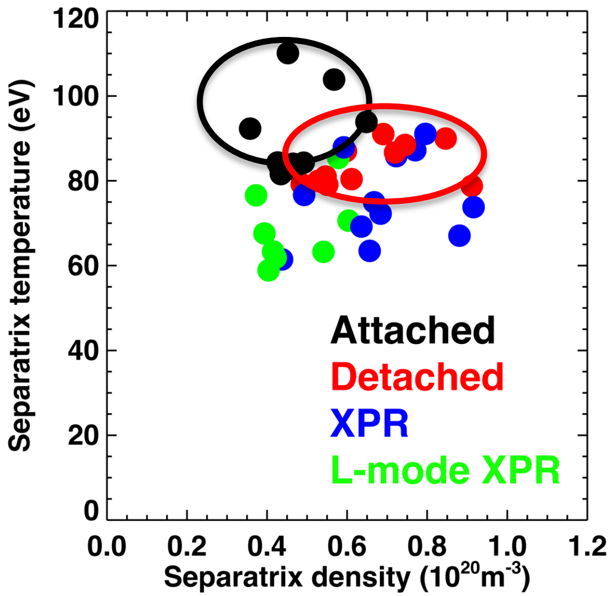

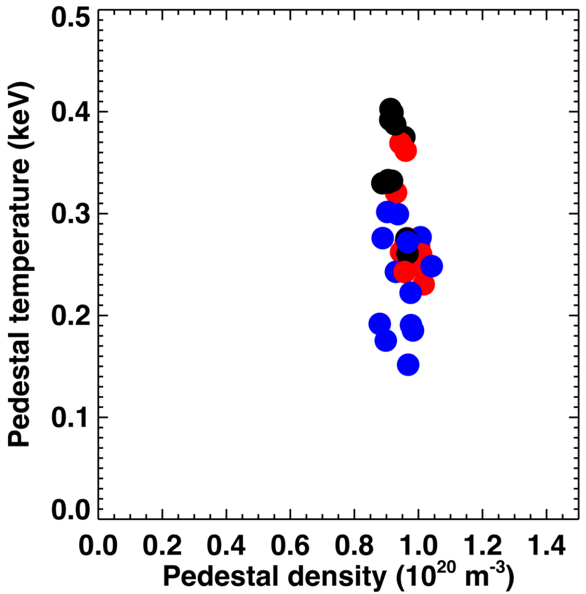

X-point radiation access with reduced pedestal and separatrix T_e, unchanged pedestal density but higher separatrix density

- Database of pedestal and separatrix values assembled across detached and XPR conditions in this experiment
    - Uncertainty in LCFS localization affects $n_{e\text{-}sep}$, $T_{e\text{-}sep}$ determination in XPR conditions

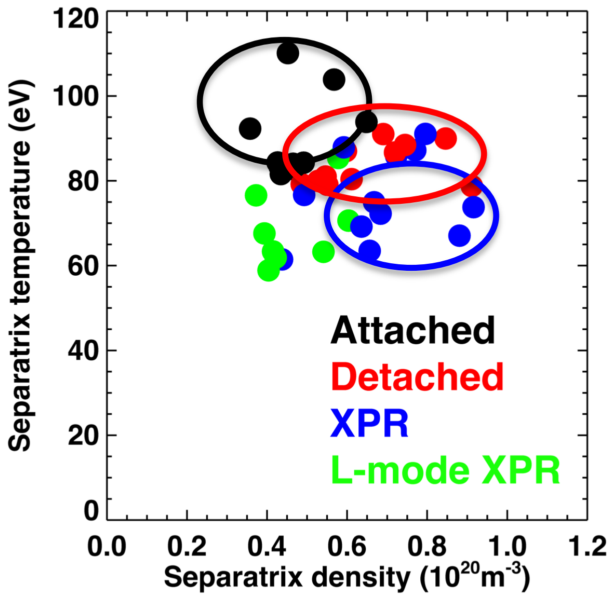

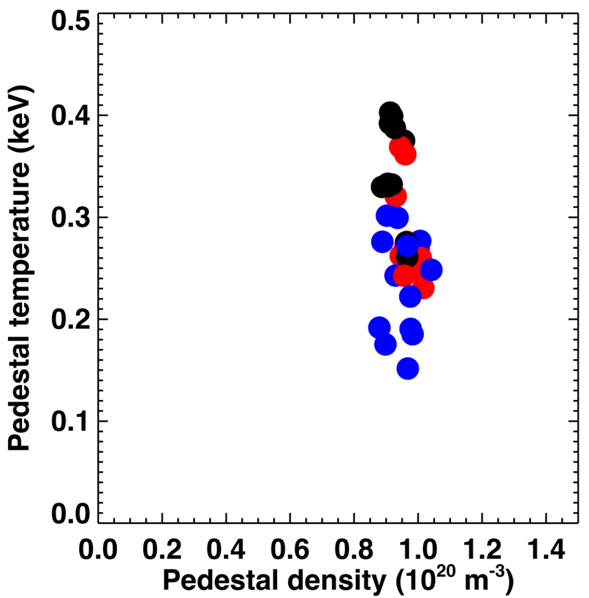

X-point radiation access with reduced pedestal and separatrix T_e, unchanged pedestal density but higher separatrix density

- Database of pedestal and separatrix values assembled across detached and XPR conditions in this experiment
  - Uncertainty in LCFS localization affects $n_{e\text{-}sep}$, $T_{e\text{-}sep}$ determination in XPR conditions

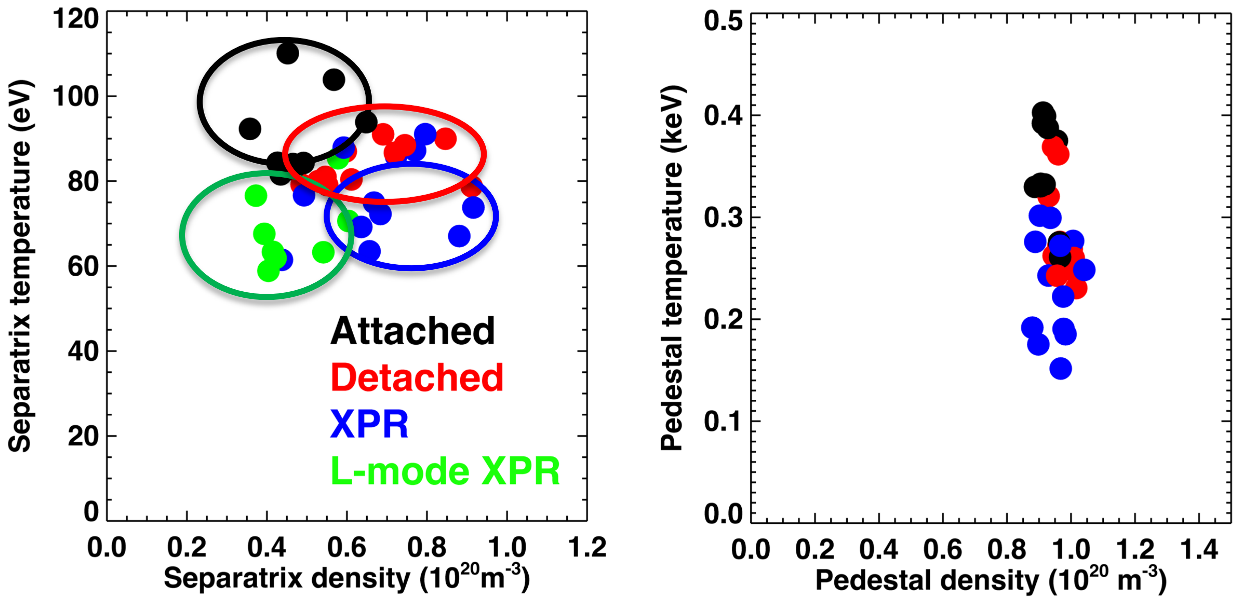

X-point radiation access with reduced pedestal and separatrix T_e, unchanged pedestal density but higher separatrix density

- Database of pedestal and separatrix values assembled across detached and XPR conditions in this experiment
  - Uncertainty in LCFS localization affects $n_{e\text{-}sep}$, $T_{e\text{-}sep}$ determination in XPR conditions

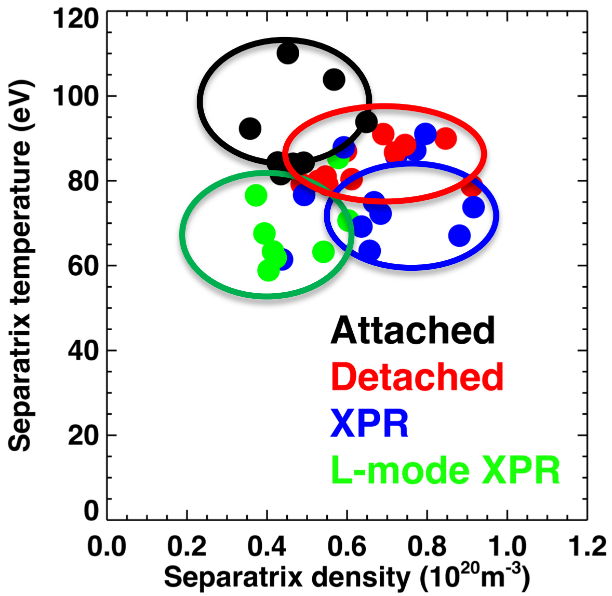

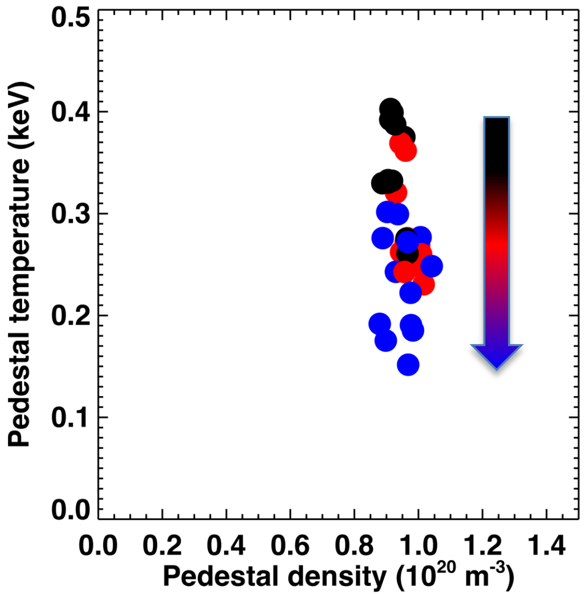

X-point radiation access with reduced pedestal and separatrix T_e, unchanged pedestal density but higher separatrix density

- Database of pedestal and separatrix values assembled across detached and XPR conditions in this experiment
  - Uncertainty in LCFS localization affects $n_{e\text{-}sep}$, $T_{e\text{-}sep}$ determination in XPR conditions
- Significant dilution at pedestal top observed in XPR conditions

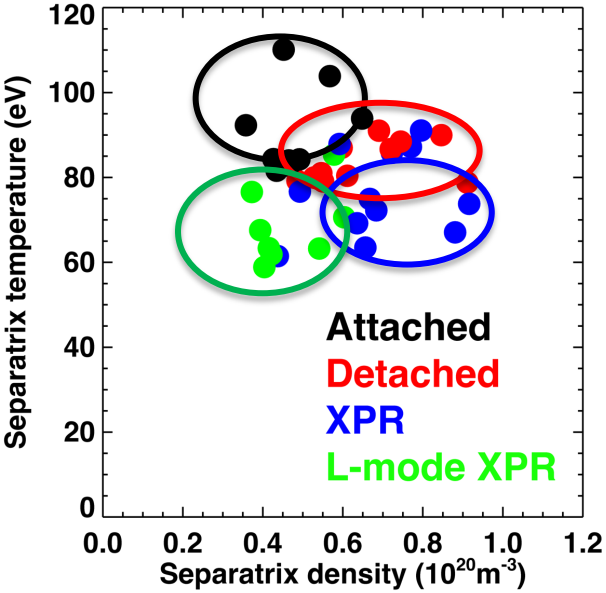

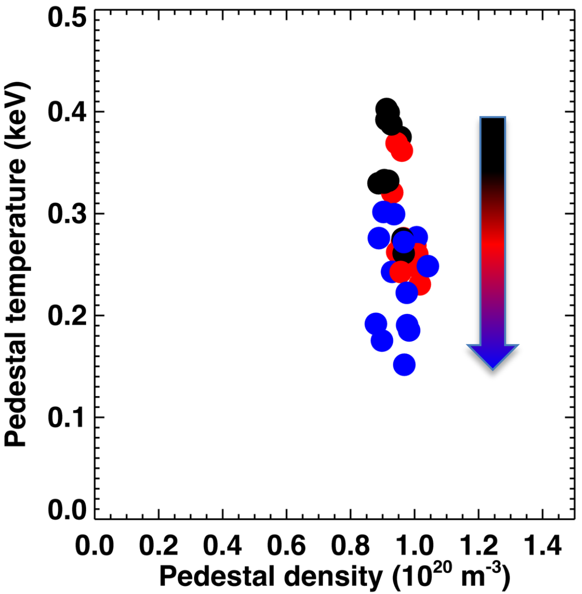

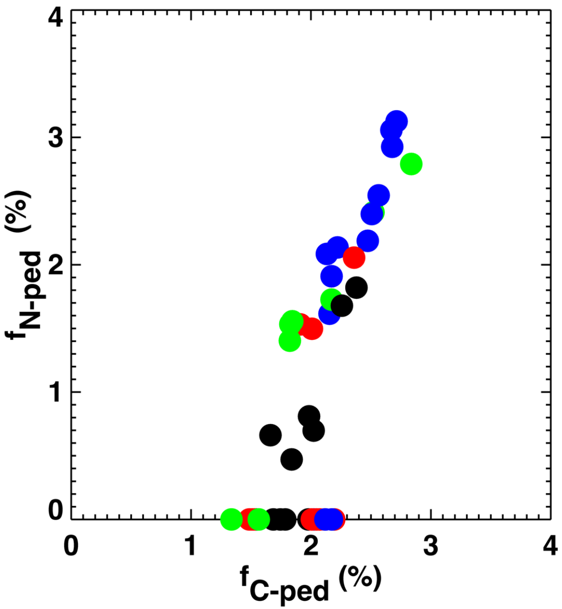

X-point radiation access with reduced pedestal and separatrix T_e, unchanged pedestal density but higher separatrix density

- Database of pedestal and separatrix values assembled across detached and XPR conditions in this experiment
  - Uncertainty in LCFS localization affects $n_{e\text{-}sep}$, $T_{e\text{-}sep}$ determination in XPR conditions
- Significant dilution at pedestal top observed in XPR conditions

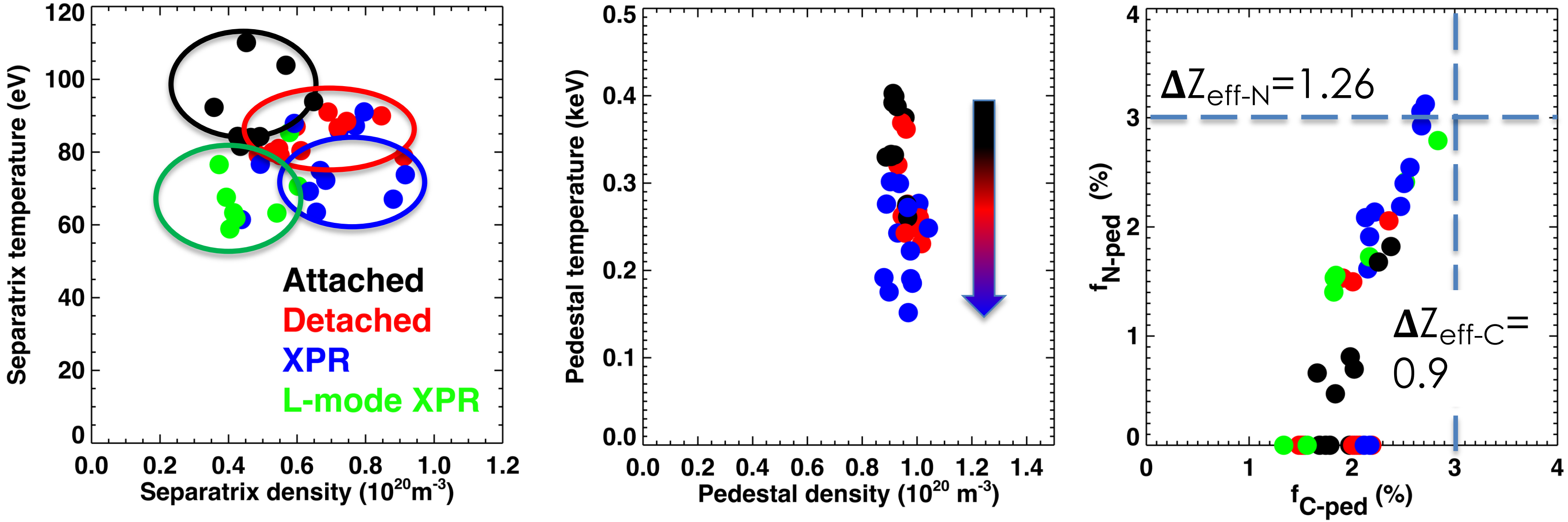

X-point radiation region accompanied by low T_e and pressure loss downstream of peak radiation in confined plasma

- T_e, n_e, p_e profiles compared in confined plasma upstream and at X-point location

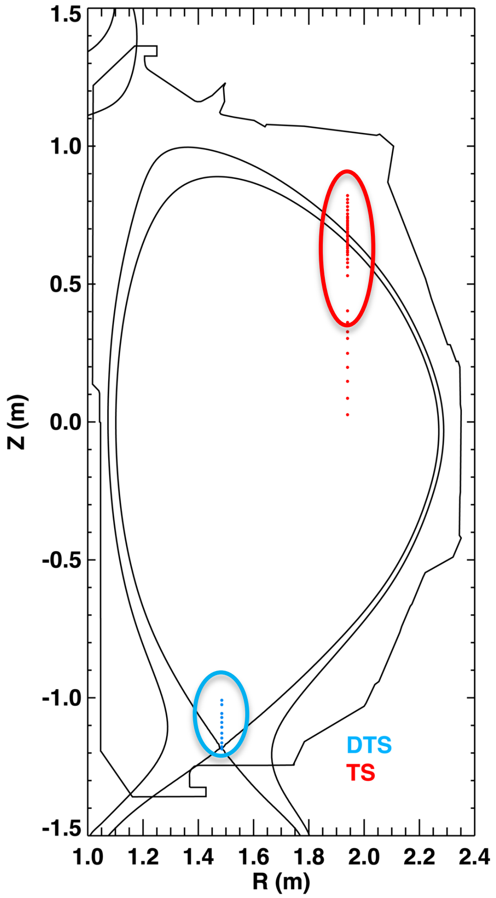

X-point radiation region accompanied by low T_e and pressure loss downstream of peak radiation in confined plasma

- T_e, n_e, p_e profiles compared in confined plasma upstream and at X-point location
- In attached conditions, T_e and p_e profiles well matched

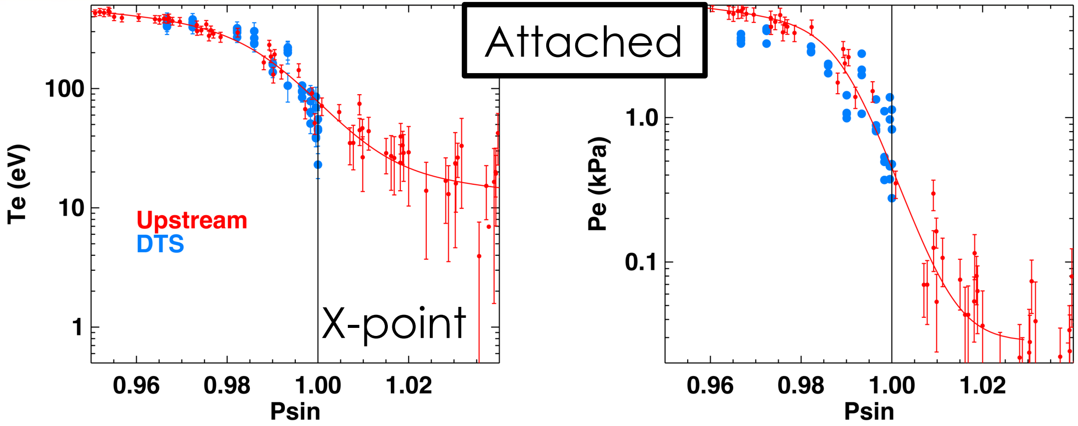

X-point radiation region accompanied by low T_e and pressure loss downstream of peak radiation in confined plasma

- T_e, n_e, p_e profiles compared in confined plasma upstream and at X-point location
- In attached conditions, T_e and p_e profiles well matched
- X-point T_e degradation observed in detached conditions

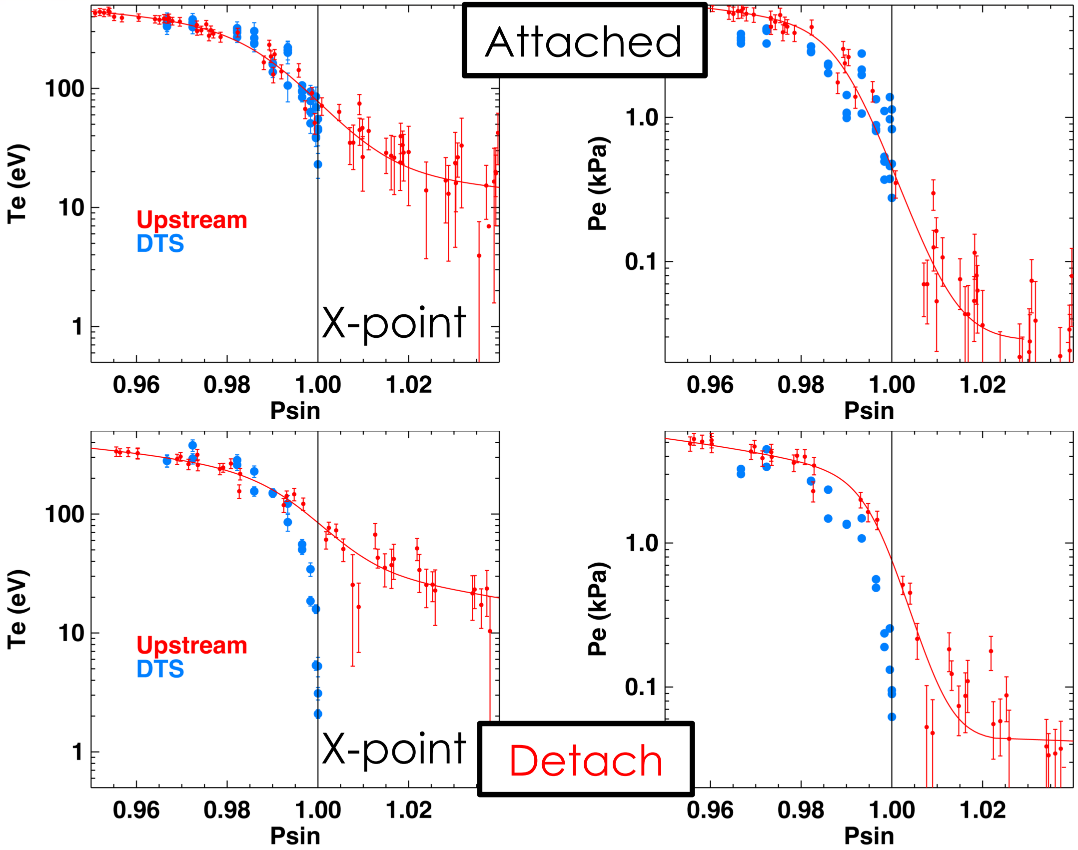

X-point radiation region accompanied by low T_e and pressure loss downstream of peak radiation in confined plasma

- T_e, n_e, p_e profiles compared in <u>confined plasma</u> upstream and at X-point location
- In attached conditions, T_e and p_e profiles well matched
- X-point T_e degradation observed in detached conditions
- X-point radiation condition have extended region of low-T_e, with pressure loss downstream of peak P_{rad} region

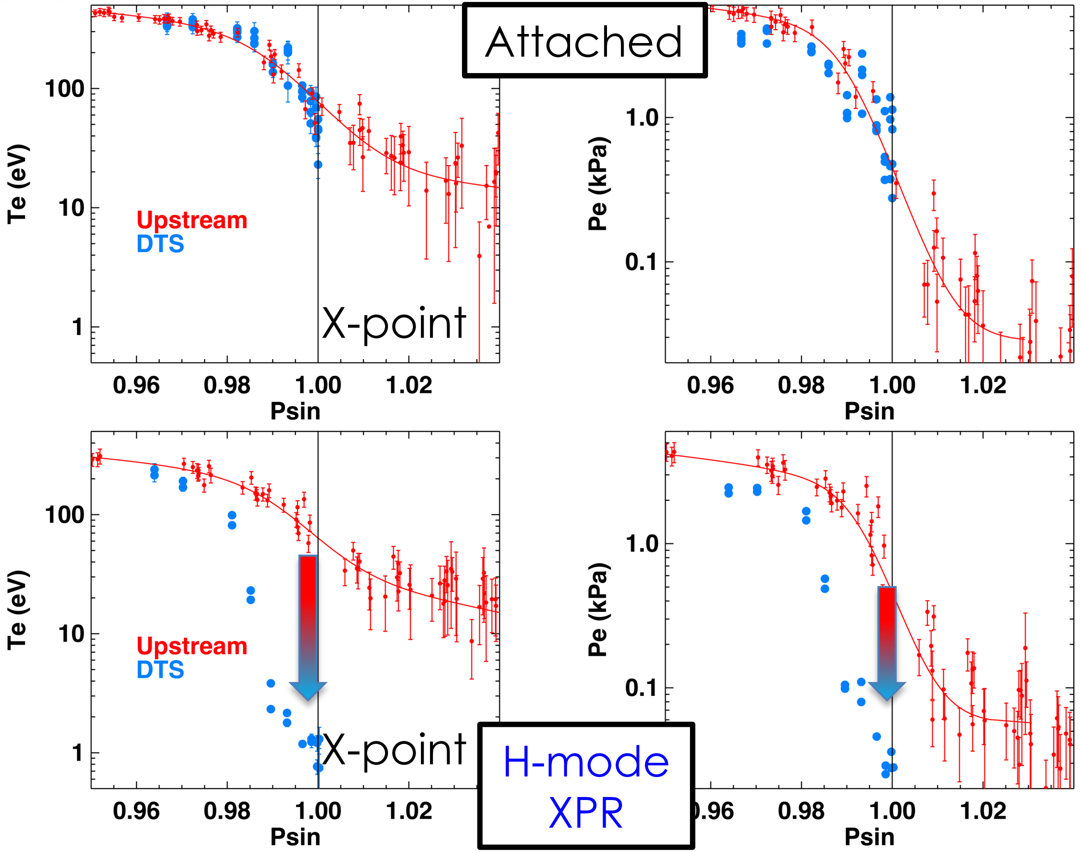

DIII-D NATIONAL FUSION FACILITY

X-point radiation region accompanied by low T_e and pressure loss downstream of peak radiation in confined plasma

- T_e, n_e, p_e profiles compared in confined plasma upstream and at X-point location
- In attached conditions, T_e and p_e profiles well matched
- X-point T_e degradation observed in detached conditions
- X-point radiation condition have extended region of low-T_e, with pressure loss downstream of peak P_{rad} region

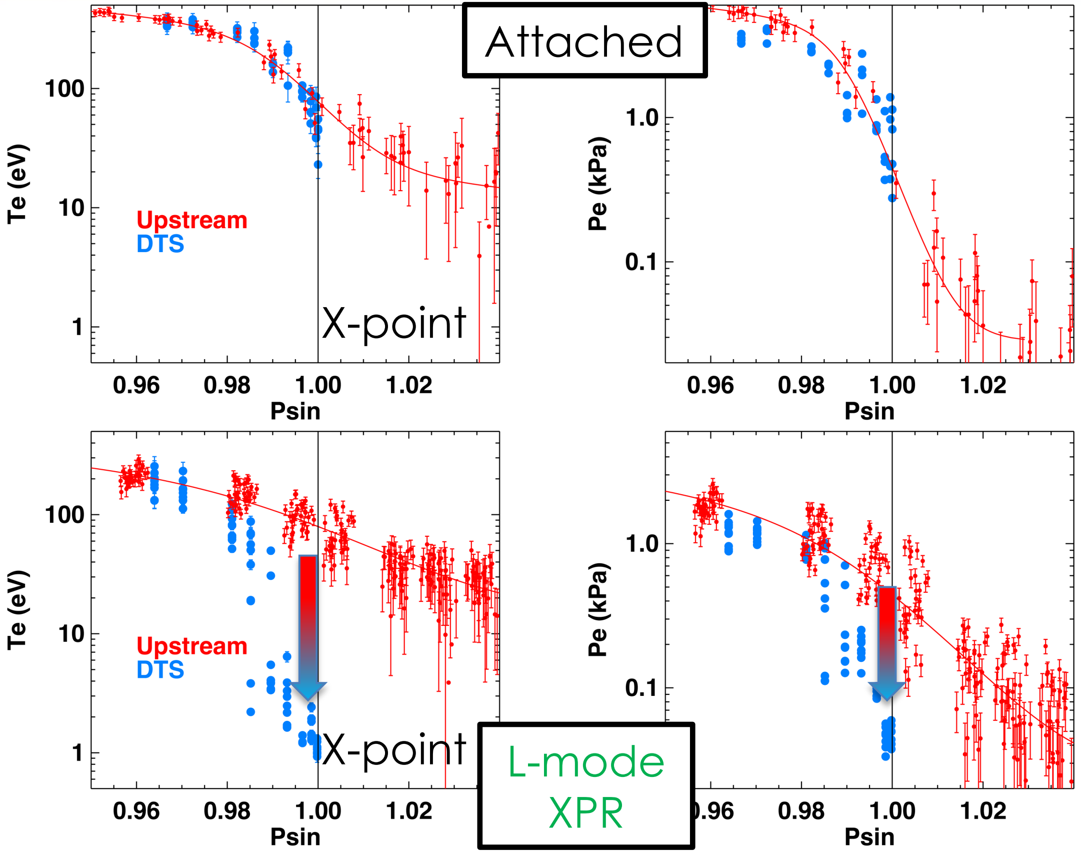

C III and radiated power reconstructions show peak emissivity/radiated power density move to inside of X-point in ELM mitigated phase of discharge

- Typical evolution of radiation front:
  1. Detached inner leg, attached outer leg
  2. Detachment cliff of outer leg
  3. Gradual transition to XPR with C III radiation occupying entire X-point region
  4. Back-transition to L-mode with stronger localized C III emission

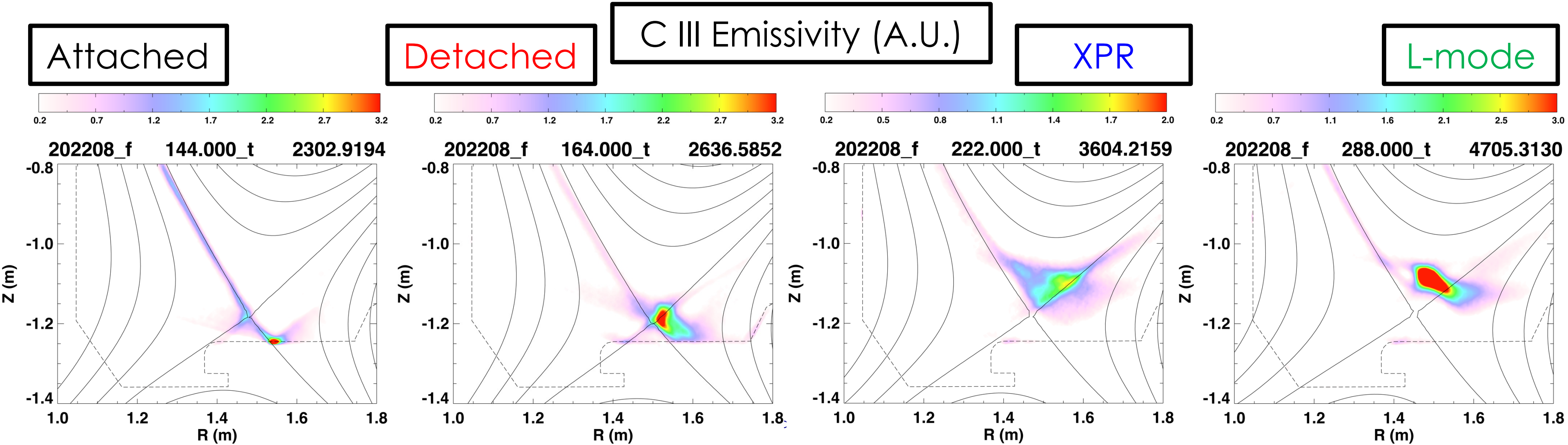

C III and radiated power reconstructions show peak emissivity/radiated power density move to inside of X-point in ELM mitigated phase of discharge

- Typical evolution of radiation front:
  1. Detached inner leg, attached outer leg
  2. Detachment cliff of outer leg
  3. Gradual transition to XPR with C III radiation occupying entire X-point region
  4. Back-transition to L-mode with stronger localized C III emission
- Consistent emissivity reconstructed from bolometer and tangential imaging

Attached | Detached | $P_{rad}(MW/m^3)$ | XPR | L-mode

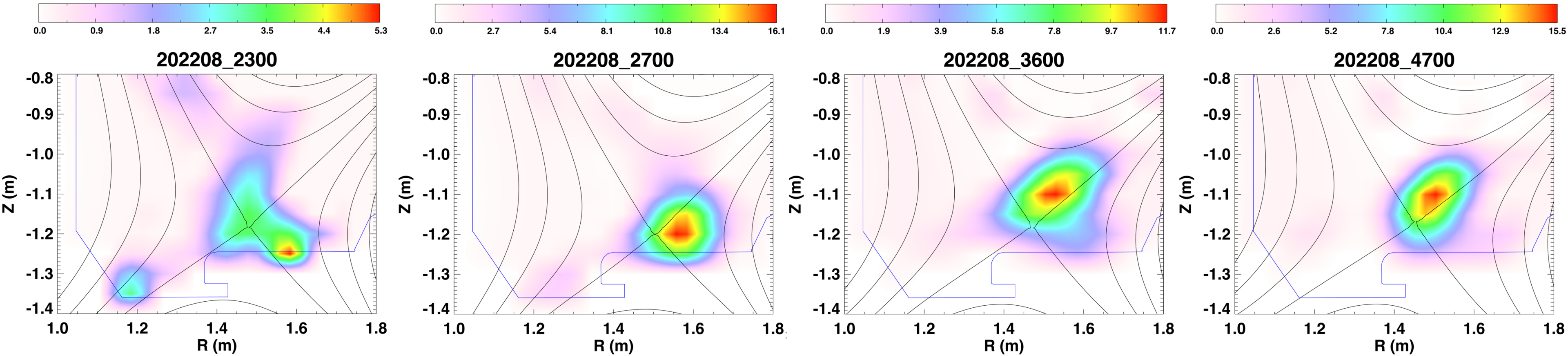

XPR dynamics: Gradual transition into X-point radiation from detachment conditions, X-point radiation front modulated by ELMs

- After detachment cliff, continuous evolution of radiation front into XPR towards LFS indicates controllability of XPR radiation front

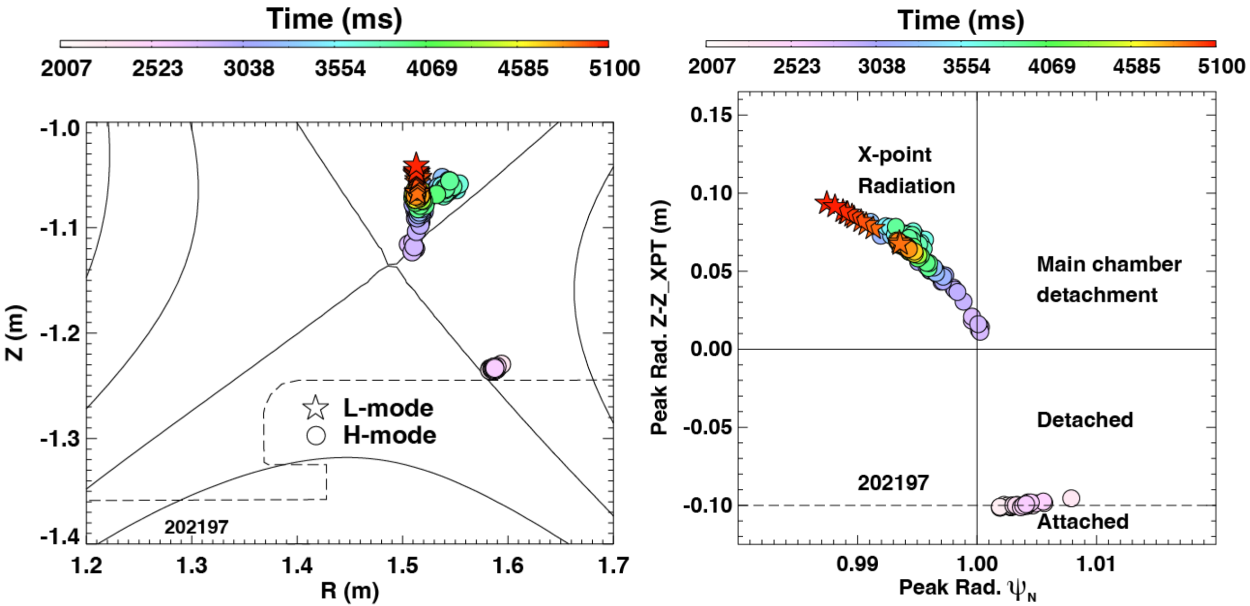

XPR dynamics: Gradual transition into X-point radiation from detachment conditions, X-point radiation front modulated by ELMs

- After detachment cliff, continuous evolution of radiation front into XPR towards LFS indicates controllability of XPR radiation front

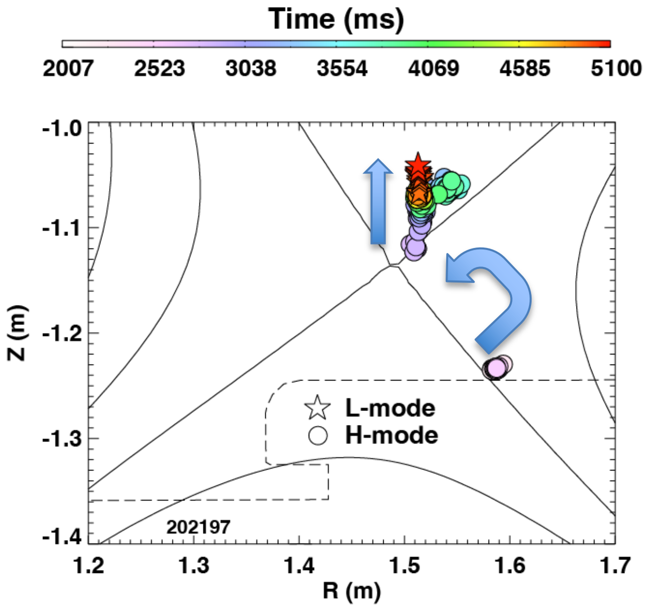

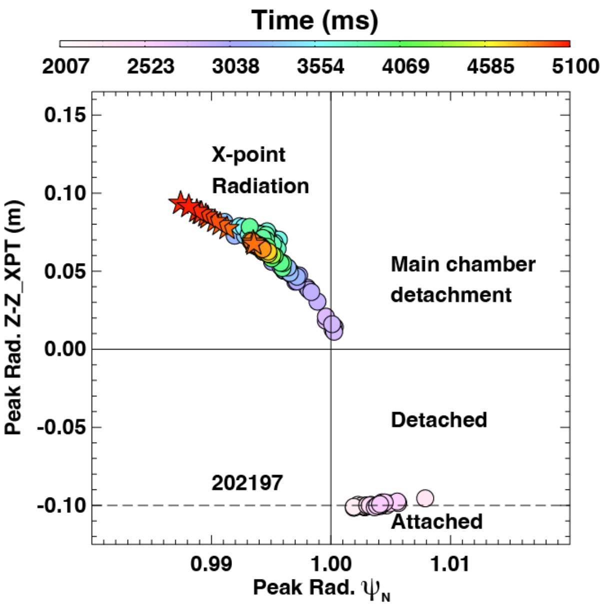

XPR dynamics: Gradual transition into X-point radiation from detachment conditions, X-point radiation front modulated by ELMs

- After detachment cliff, continuous evolution of radiation front into XPR towards LFS indicates controllability of XPR radiation front
- Modulation of radiation front within confined plasma observed due to interaction with ELMs
  - Broadens bolometry reconstructed emissivity

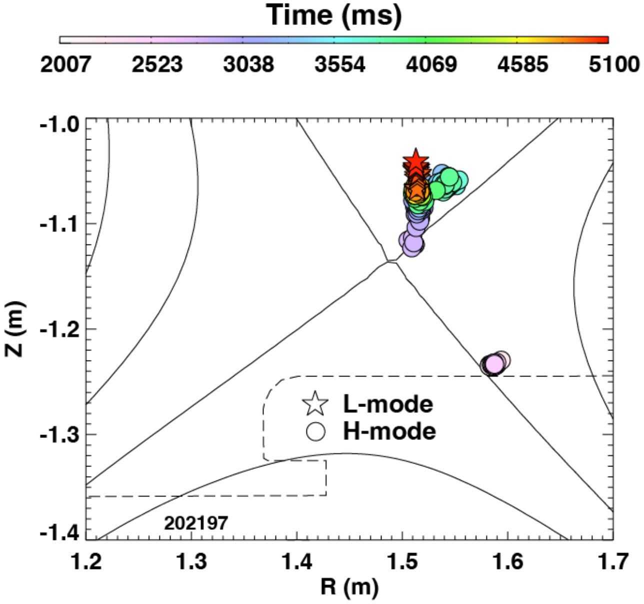

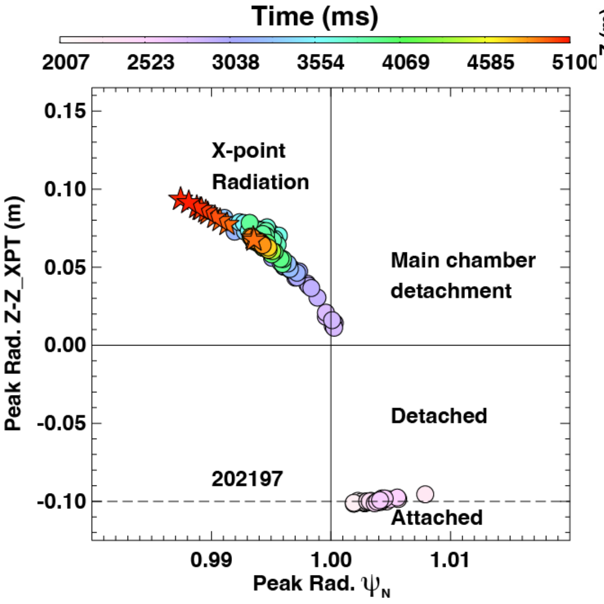

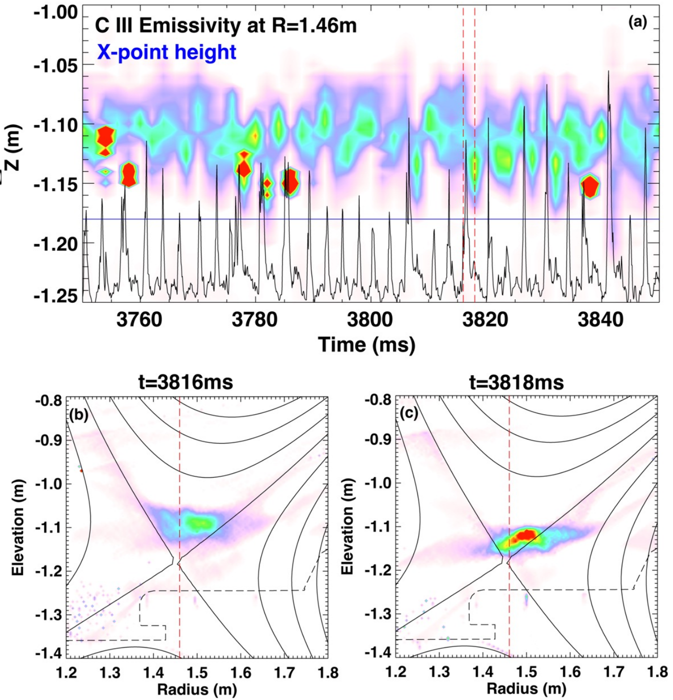

Partial, deep detachment observed during XPR phase, residual particle flux in far SOL

- Deep (DOD~10) detachment at strike point during XPR phase
    - Residual particle flux in near/far SOL (different from closed divertor [Ma IAEA25])
- Particle flux reduced ~2x compared to detached case
- OSP heat flux mitigated to baseline level

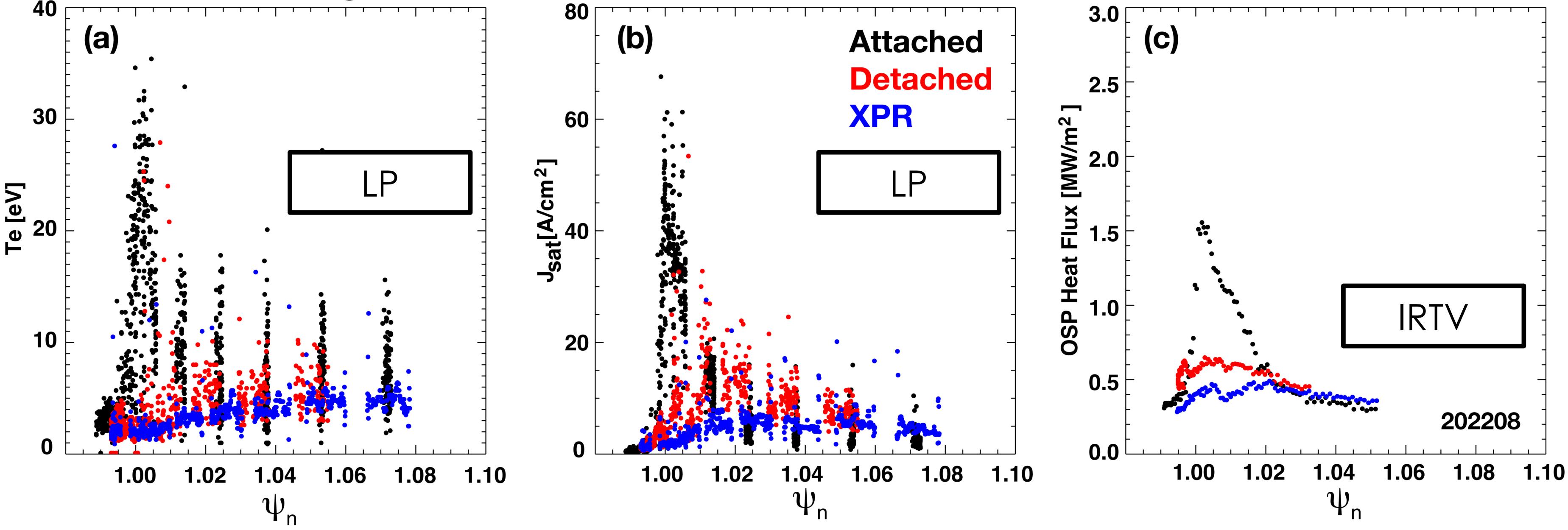

Total radiated power fractions 80-95% with, core radiated power fractions up to 55% during XPR phases

- F_{rad} (core, tot) inferred from P_{rad} (core, tot) from bolometer reconstruction to injected (Ohmic + auxiliary) power
- XPR enables marginally higher F_{rad} (tot) at twice higher F_{rad} (core)
- Movement of radiated power density inside separatrix lowers $T_{e\text{-}ped}$ and enables access to ELM mitigated scenarios

- Discontinuity in $F_{rad\text{-}core}$ artifact
- $F_{rad\text{-}core}$ can be lower bound of actual $F_{rad\text{-}core}$ due to bolometer resolution

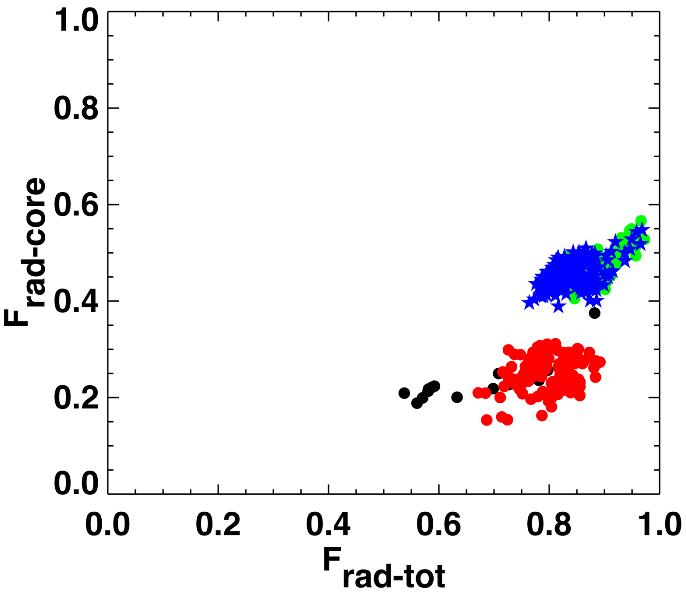

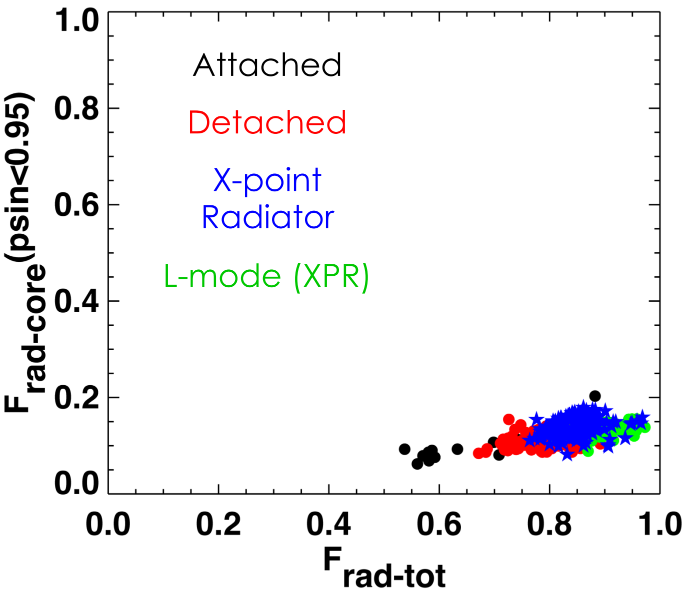

Mitigation in ELM size, improved ELM buffering with only marginal reduction in total power lost through ELMs observed in XPR phase

- ELM size reduced from 1-2% of stored energy to 0.4% in XPR phase
- Higher frequency ELMs (100Hz →3-400Hz) lead to only marginal reduction in total energy lost through ELMs but with reduced peak heat fluxes

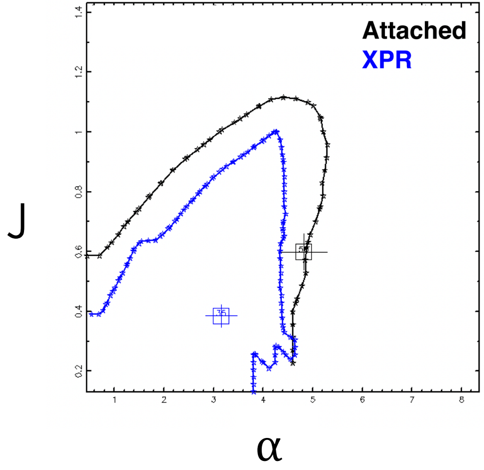

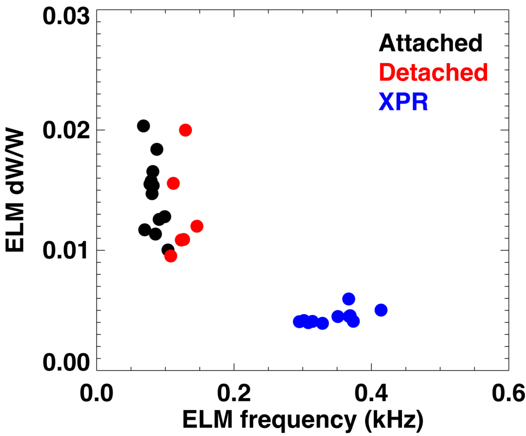

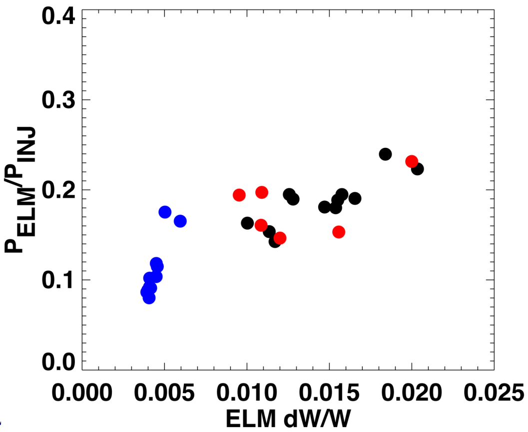

DIII-D NATIONAL FUSION FACILITY

Mitigation in ELM size, improved ELM buffering with only marginal reduction in total power lost through ELMs observed in XPR phase

- ELM size reduced from 1-2% of stored energy to 0.4% in XPR phase
- Higher frequency ELMs (100Hz →3-400Hz) lead to only marginal reduction in total energy lost through ELMs but with reduced peak heat fluxes
- Reduced accounted energy in outer divertor per ELM size in XPR phase indicates possible improved buffering

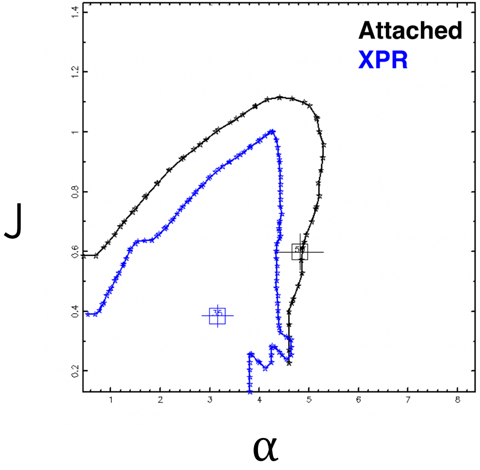

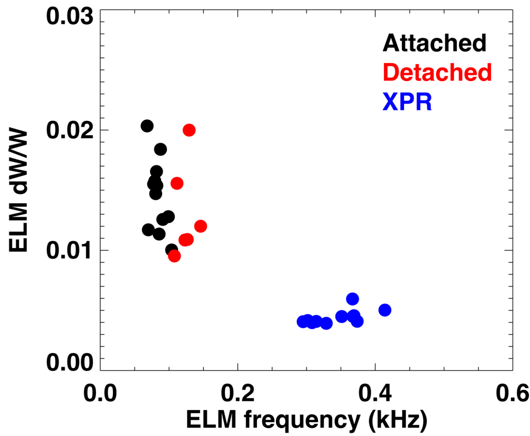

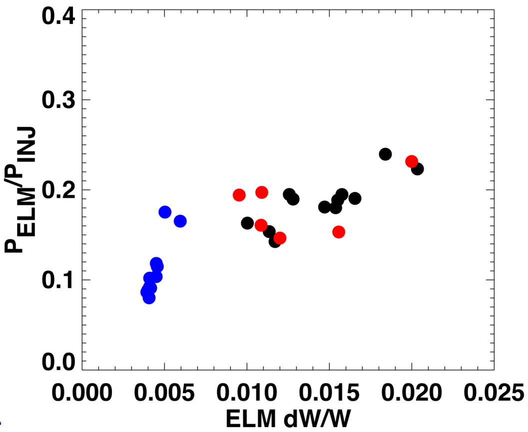

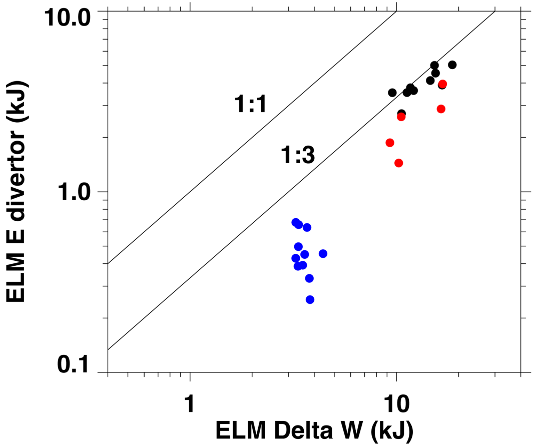

Trade-off between ELM mitigation and confinement degradation beyond detachment with reduction in confinement up to 20%

- Penetration of radiation front in confined plasma associated with mitigation of ELMs
- Concomitant reduction in normalized plasma pressure up to 20%
- Similar confinement degradation and ELM-mitigation observed with XPR in advanced tokamak regimes, with higher performance core offsetting overall confinement loss

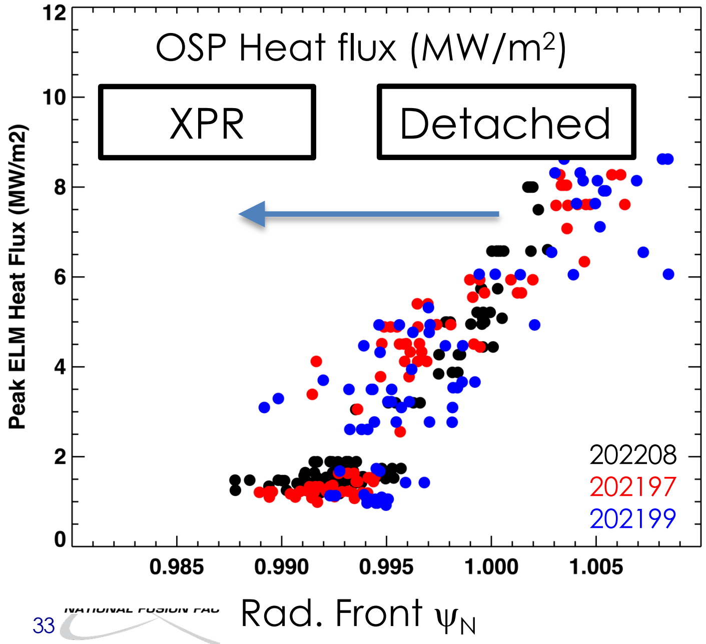

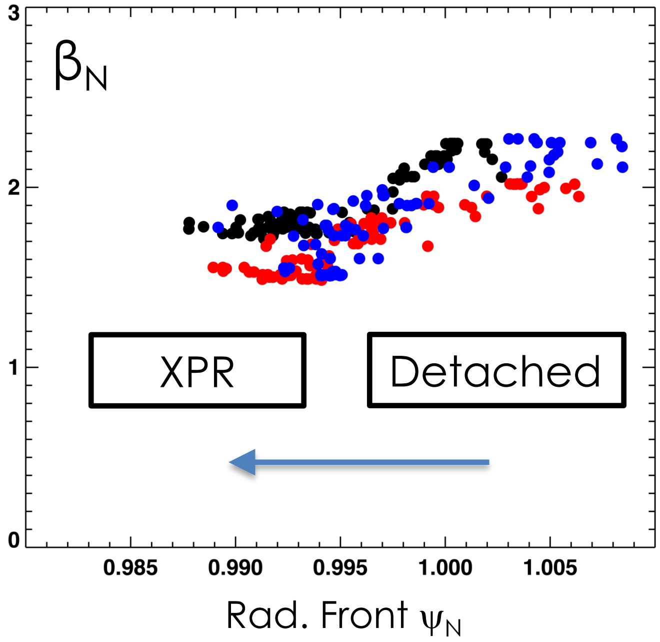

Trade-off between ELM mitigation and confinement degradation beyond detachment with reduction in confinement up to 20%

- Penetration of radiation front in confined plasma associated with mitigation of ELMs
- Concomitant reduction in normalized plasma pressure up to 20%
- Similar confinement degradation and ELM-mitigation observed with XPR in advanced tokamak regimes, with higher performance core offsetting overall confinement loss

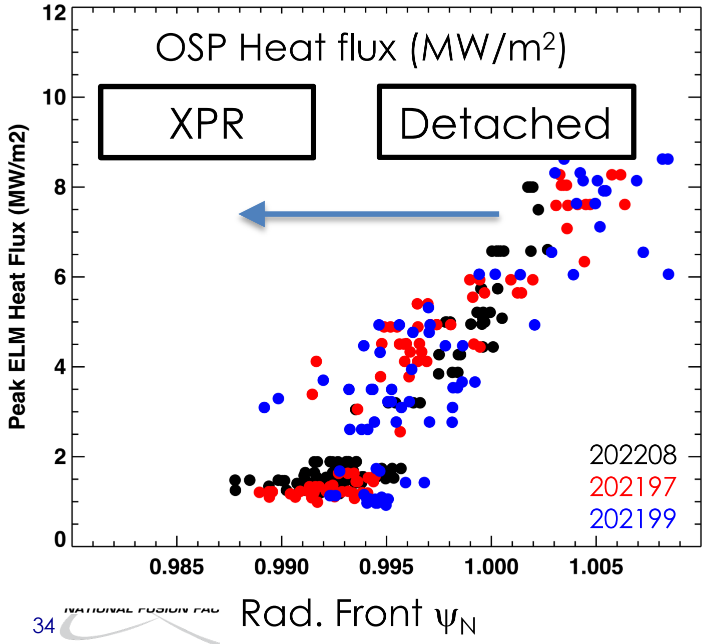

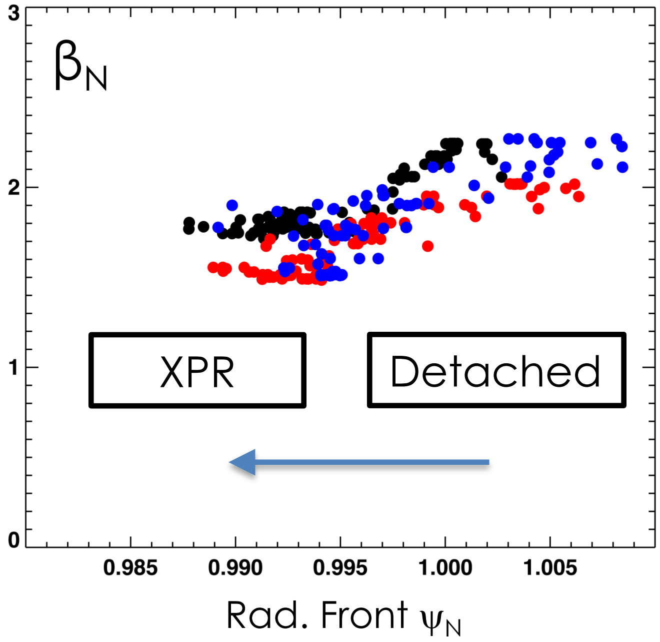

Conclusions

- Stable XPR with both C and N dominated XPR enabled detailed measurements of plasma parameters and radiating species in X-point region
- After fast detachment transition, continuous XPR evolution indicates controllability
- Movement of radiated power density inside LCFS lowers $T_{e\text{-}ped}$ and enables access to ELM mitigated scenarios
- Mitigation of ELMs and improved buffering is obtained in XPR phase with trade off of degraded confinement and dilution

Conclusions

- Stable XPR with both C and N dominated XPR enabled detailed measurements of plasma parameters and radiating species in X-point region
- After fast detachment transition, continuous XPR evolution indicates controllability
- Movement of radiated power density inside LCFS lowers $T_{e\text{-}ped}$ and enables access to ELM mitigated scenarios
- Mitigation of ELMs and improved buffering is obtained in XPR phase with trade off of degraded confinement and dilution
- Ongoing work on detailed characterization of radiative properties in X-point region and comparison to reduced [Stroth NF22] and fluid models
- Future research to focus on improving extrapolation capabilities: identify transport channels in XPR ELM-suppressed phase, requirements for ELM suppression, impact of impurities on XPR, application of XPR to advanced scenarios, multi-machine comparison

XPR dynamics: C dominated vs N dominated radiation

- Narrower window of operation with C radiation before backtransition
-

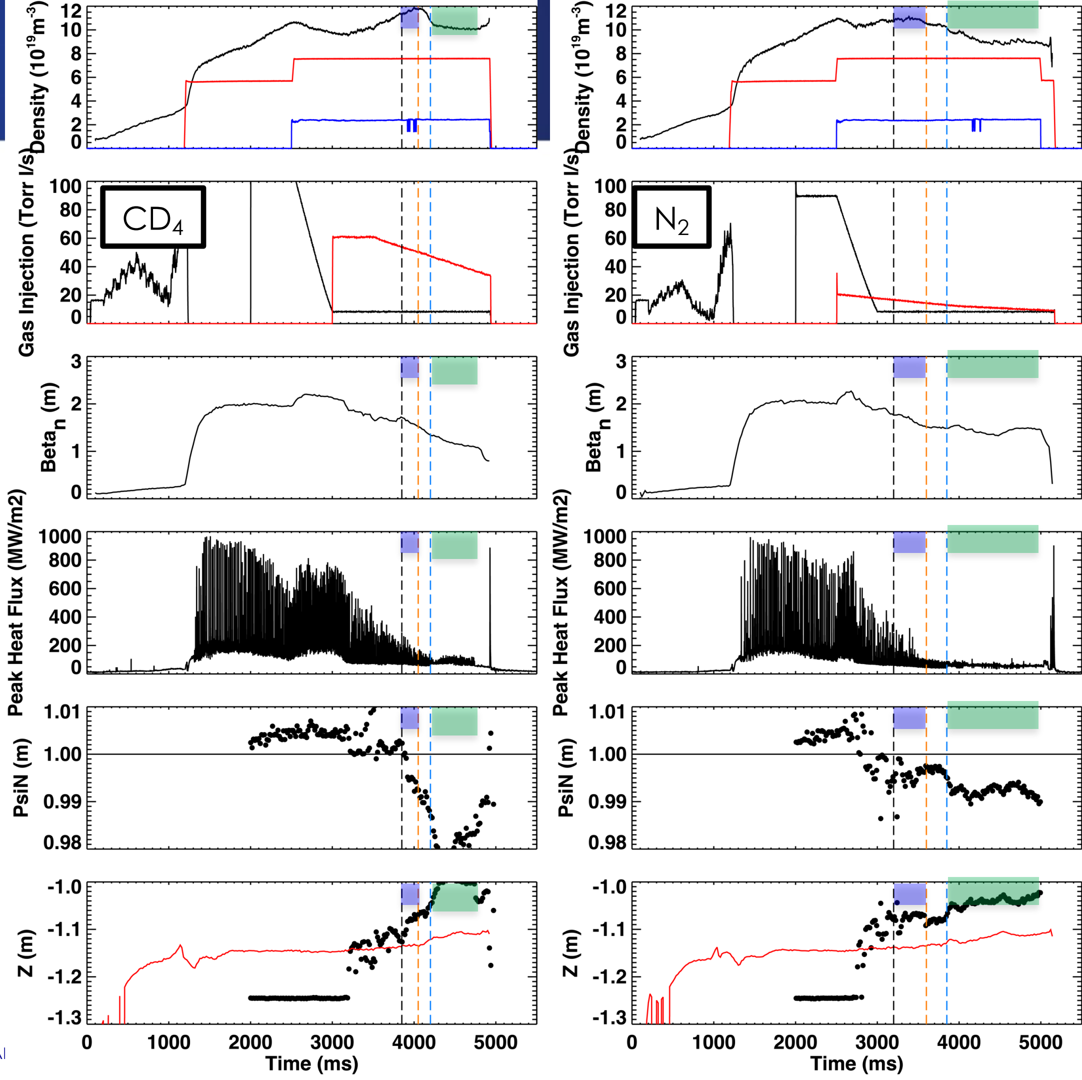

DIII-D NATIONAL FUSION FACILITY

IAI

XPR dynamics: C dominated vs N dominated radiation

- Shallower XPR with C before backtransition

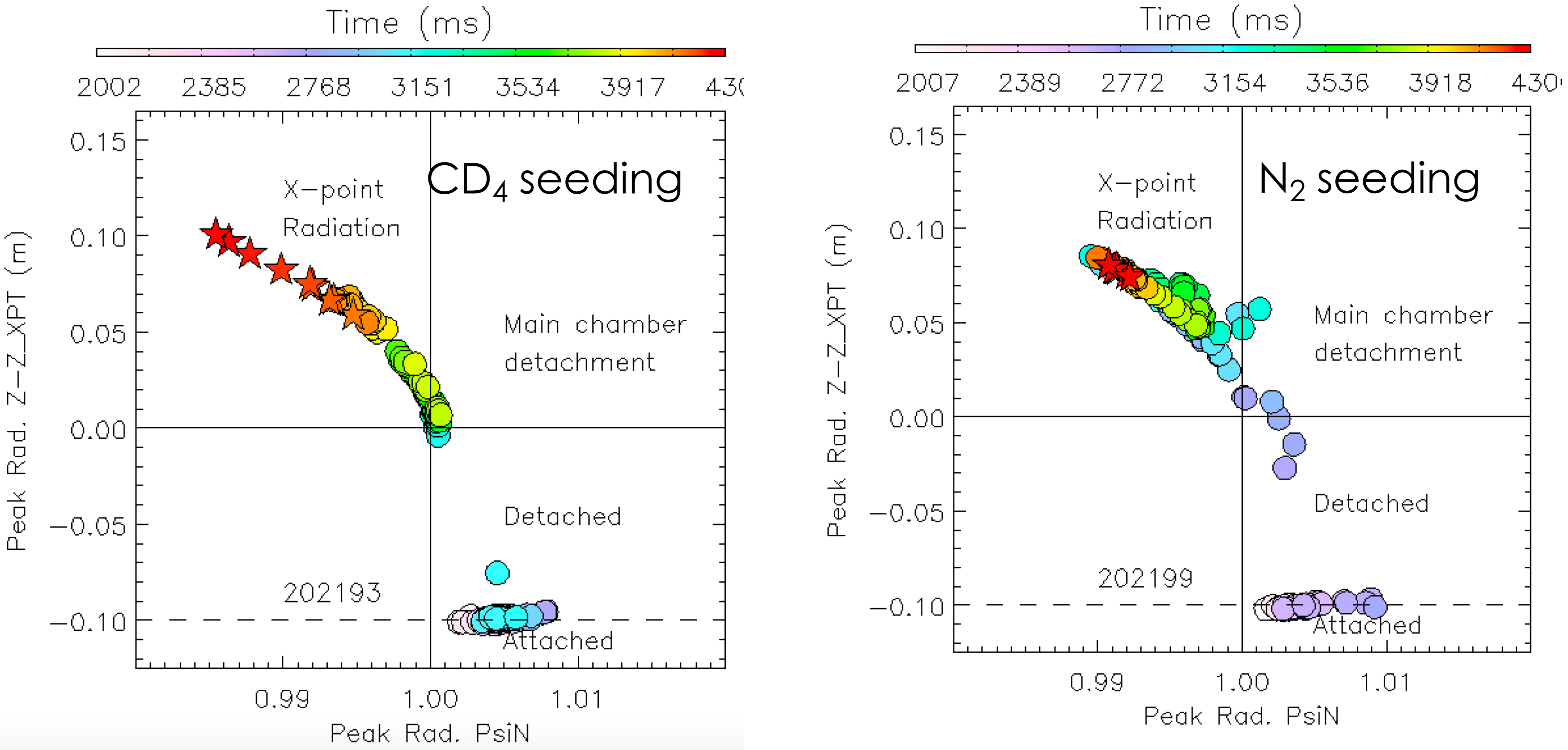

XPR dynamics: C dominated vs N dominated radiation

- VUV spectrum of resonance transition through X-point in XPR phase
- C XPR dominated by C IV, C III radiation
- N XPR, C radiation reduced by ~2X. Radiation dominated by N IV, N V

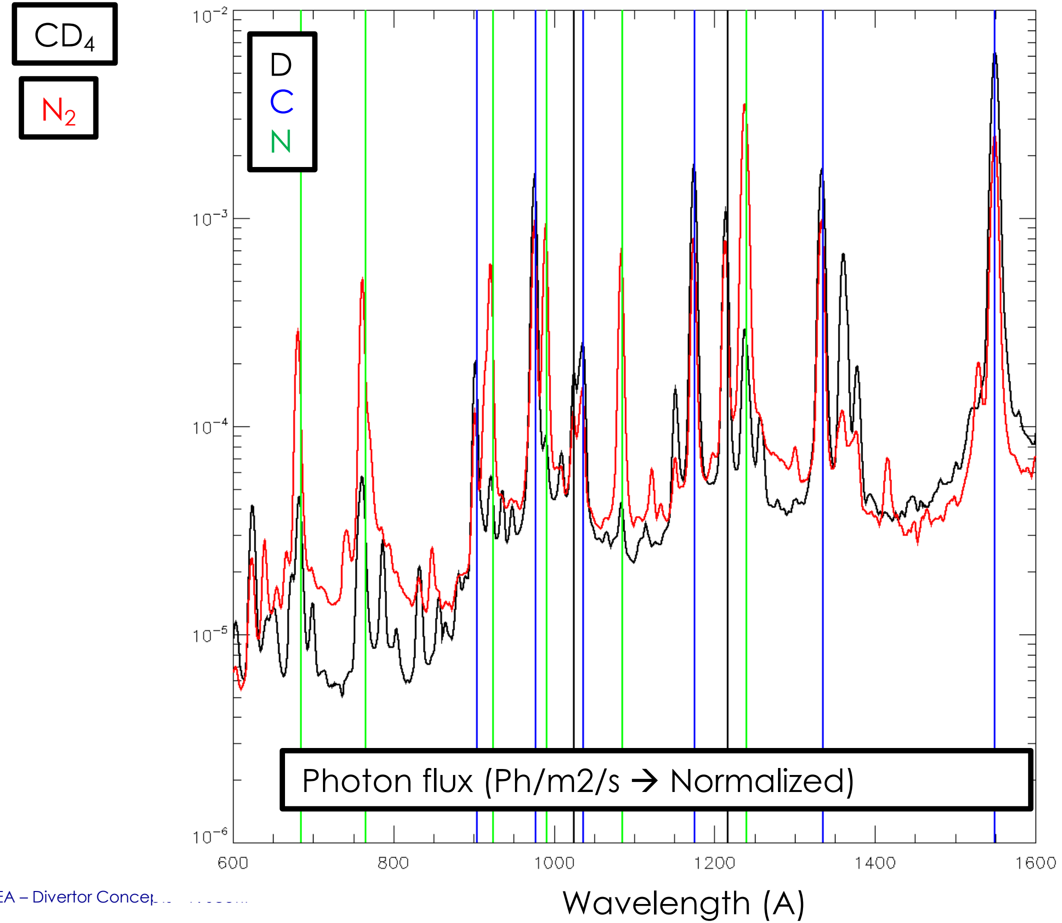

Dense (3-5x10^{20} m^{-3}), cold (1-2 eV) region observed in last 1% of ψ_n during XPR phase in both L and H mode

- T_e, n_e, p_e profiles at X-point compared for attached, detached, H-mode XPR and L-mode XPR
- L-mode XPR shows reduced pressure for $\psi_n < \psi_{n\text{-XPR}}$ and higher pressure downstream of XPR (same T_e, higher n_e) compared to H-mode XPR

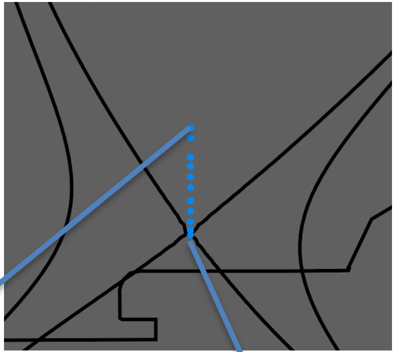

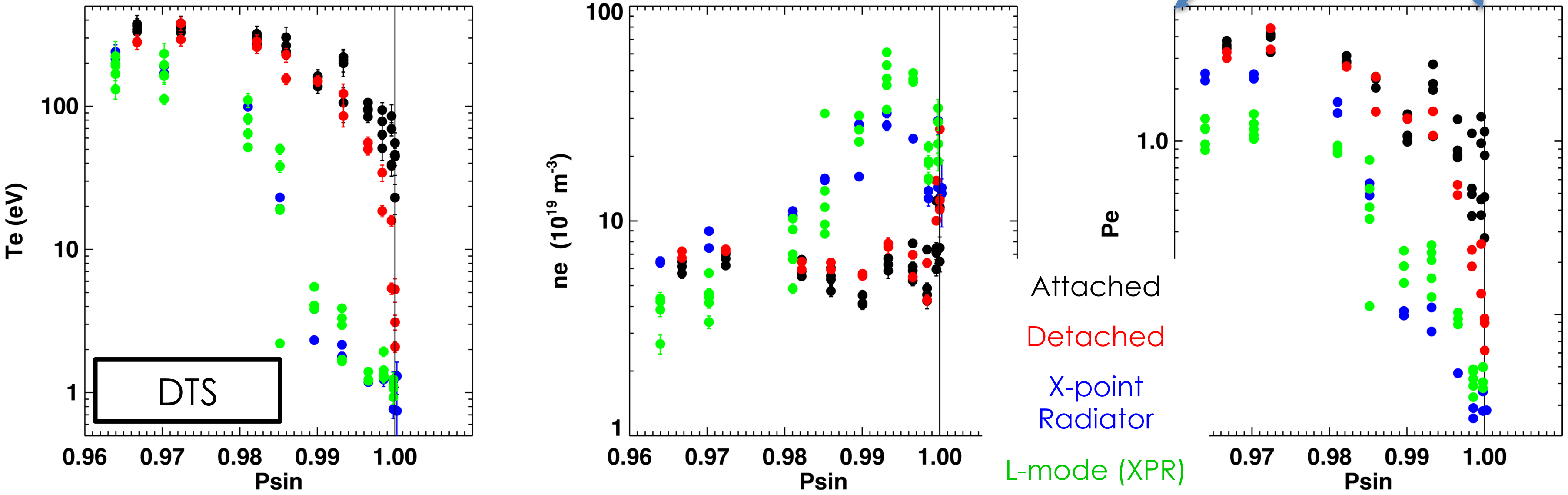

Initial UEDGE simulations with cross field drifts capture access to X-point radiation but show bifurcation and poloidally higher radiation localization

- Multi fluid UEDGE simulations with cross field drifts and fixed fraction C and N impurities performed matching experimental upstream profiles
- Access to X-point radiation via seeding and density ramps
- Fixed fraction simulation show minimal differences between C and N XPR
- Multi-charge state simulations ongoing
- n_{D0} at peak P_{rad} ~5e16

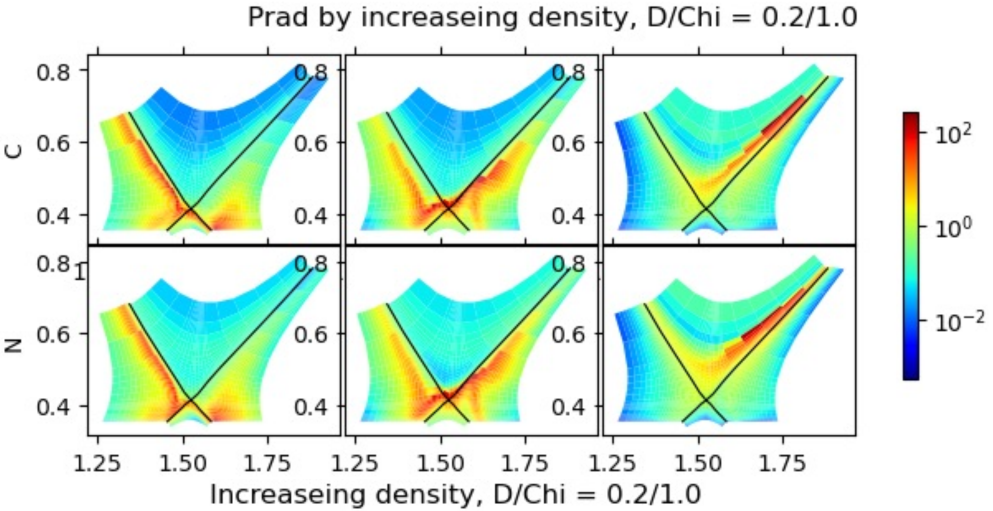

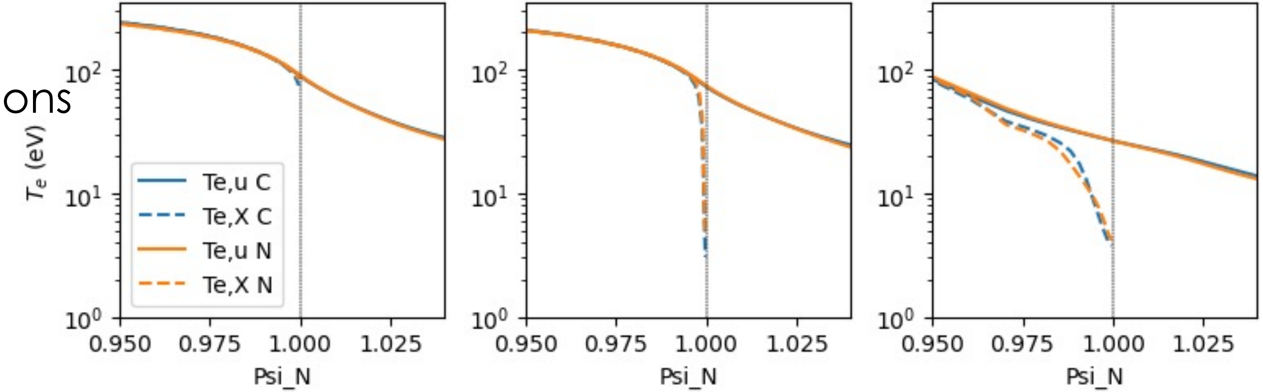

DIII-D NATIONAL FUSION FACILITY

Current scan with repeated programming

- Stable location of radiation moves to HFS at lower current
- At lower current stable radiation location only for ~0.5 s then HFS MARFE evolution

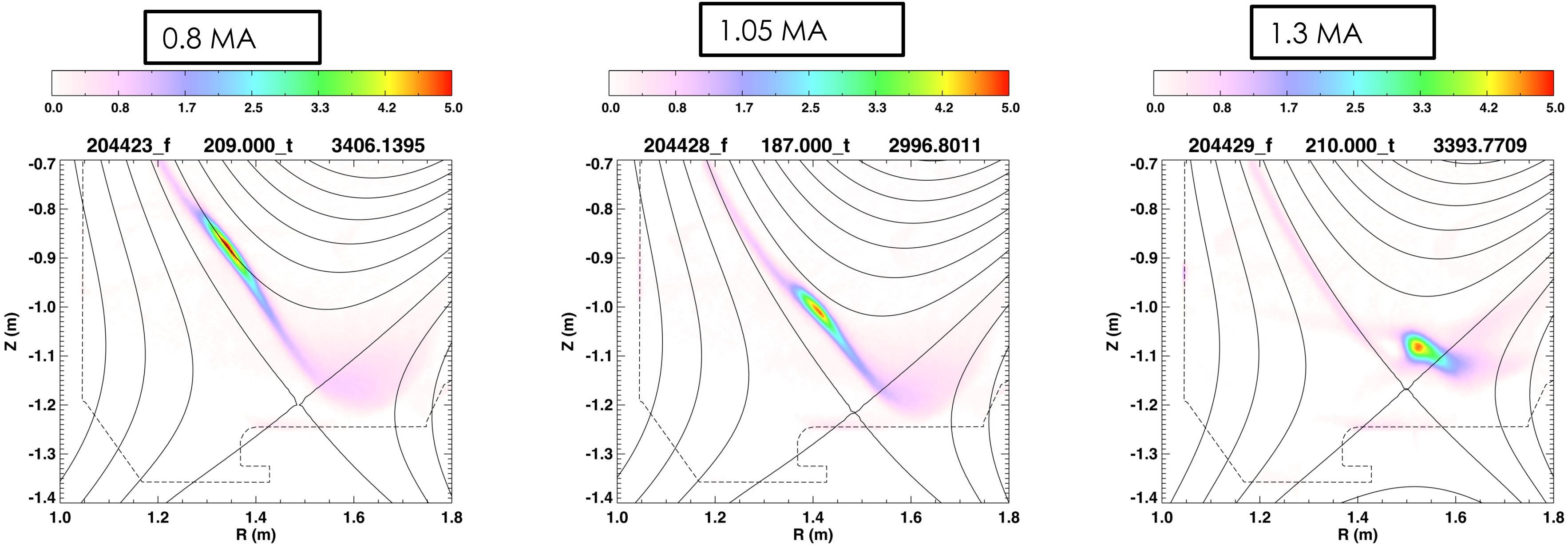

Current scan with repeated programming

- Stable location of radiation moves to HFS at lower current
- With longer $L_{//}$, unstable evolution into MARFE, consistent with model expectations

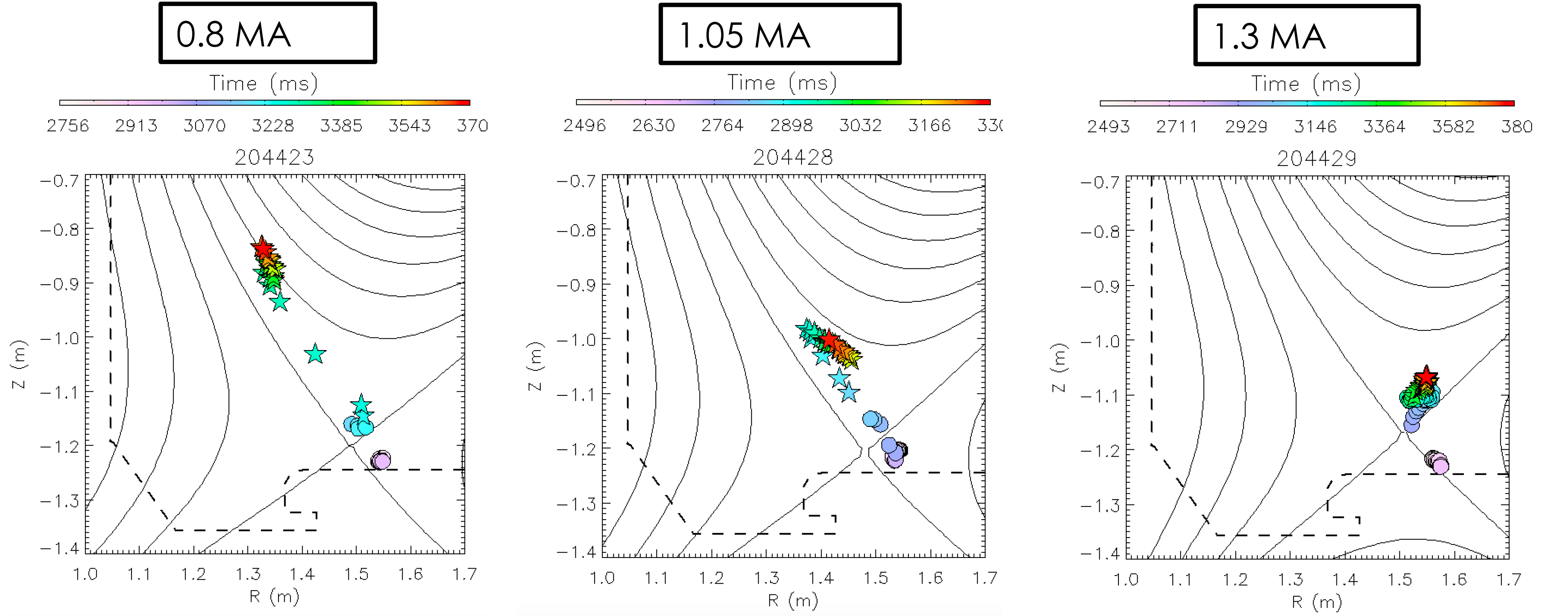

X-point height scan with repeated programming

- Similar performance and radiation evolution

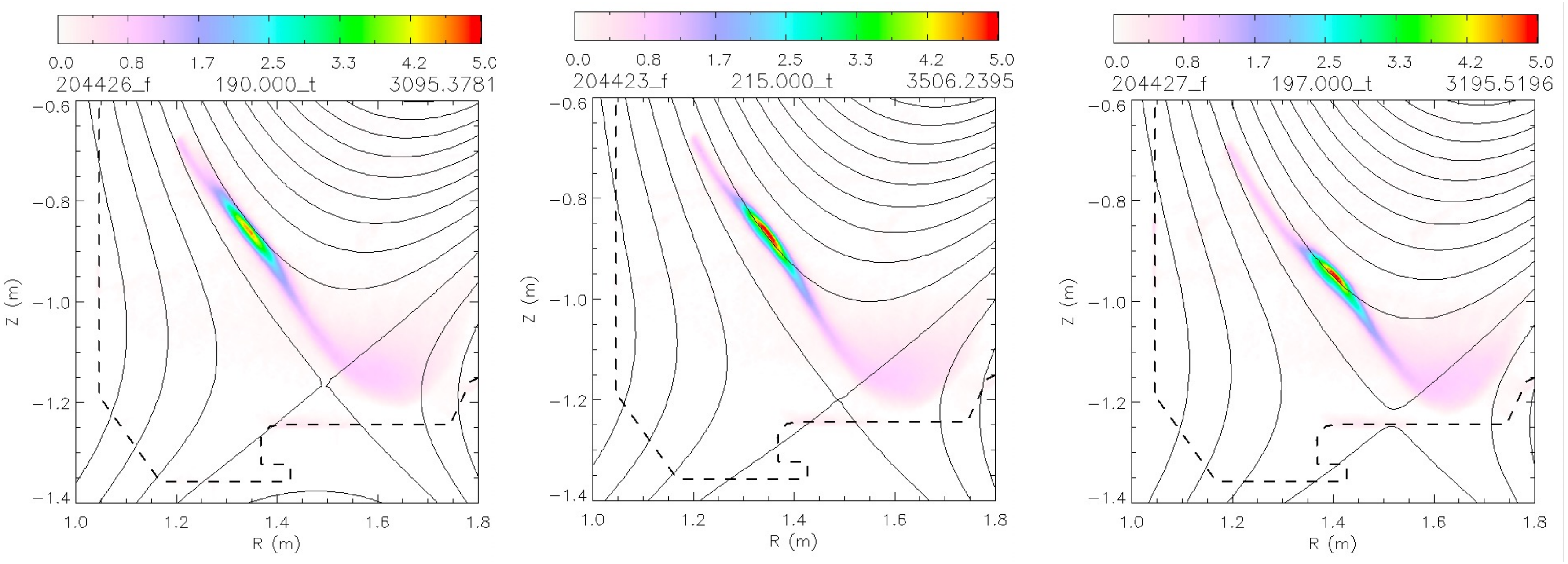

Geometry and comparison to ASDEX

AUG: H-mode, #30506 @ 5 s

P = 10 MW, $n_{sep} = 3 \times 10^{19}$ m^{-3}

DIII-D: H-mode, #202208 @ 3 s

P = 12 MW, $n_{sep} = 2 \times 10^{19}$ m^{-3}

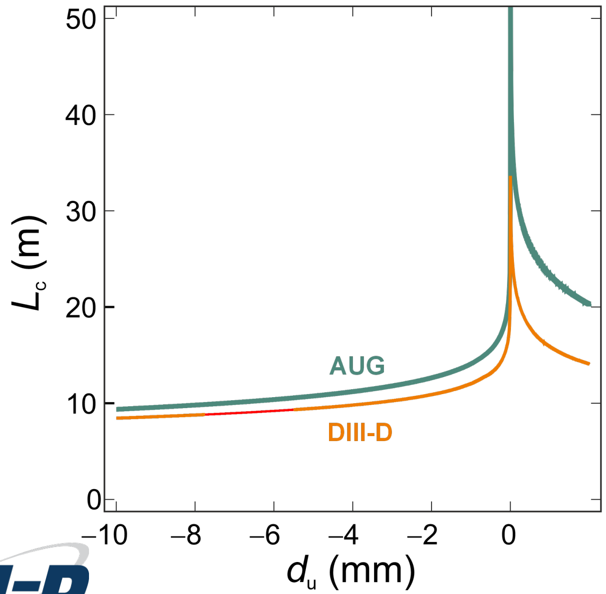

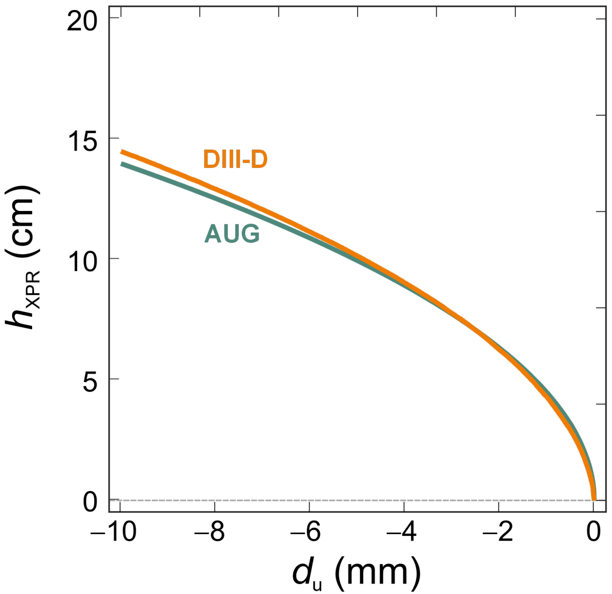

U. Stroth

Impurity mix

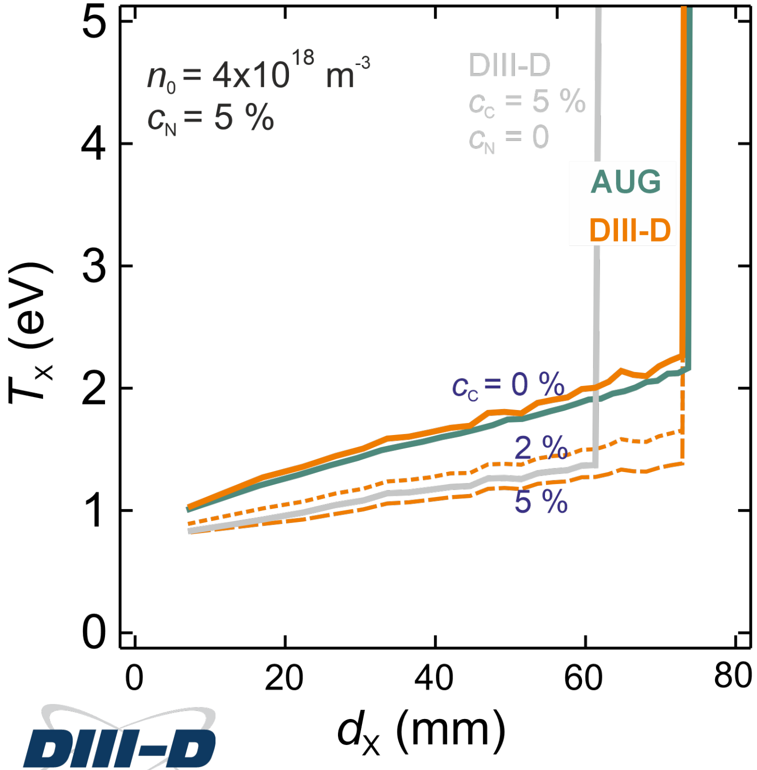

- XPR height is not affected by carbon
- XPR temperature drops below 1 eV
- With carbon only, XPR height is reduced

U. Stroth